ISTANBUL TECHNICAL UNIVERSITY ★ GRADUATE SCHOOL

COOPERATIVE VEHICULAR COMMUNICATION SYSTEMS WITH PHYSICAL LAYER SECURITY AND NOMA TECHNIQUES

M.Sc. THESIS

Semiha KOŞU

Department of Communication Systems

Satellite Communication and Remote Sensing Program

FEBRUARY 2021

ISTANBUL TECHNICAL UNIVERSITY ★ GRADUATE SCHOOL

COOPERATIVE VEHICULAR COMMUNICATION SYSTEMS WITH PHYSICAL LAYER SECURITY AND NOMA TECHNIQUES

M.Sc. THESIS

Semiha KOŞU
(705181014)

Department of Communication Systems

Satellite Communication and Remote Sensing Program

Thesis Advisor: Prof. Dr. Lütfiye DURAK ATA
Co-advisor: Dr. Serdar Özgür ATA

FEBRUARY 2021

İSTANBUL TEKNİK ÜNİVERSİTESİ ★ LİSANSÜSTÜ EĞİTİM ENSTİTÜSÜ

FİZİKSEL KATMAN GÜVENLİĞİ VE NOMA TEKNİKLERİ İLE İŞBİRLİKLİKLİ ARAÇLAR ARASI İLETİŞİM SİSTEMLERİ

YÜKSEK LİSANS TEZİ

Semiha KOŞU
(705181014)

İletişim Sistemleri Anabilim Dalı

Uydu Haberleşmesi ve Uzaktan Algılama Programı

Tez Danışmanı: Prof. Dr. Lütfiye DURAK ATA
Eş Danışman: Dr. Serdar Özgür ATA

ŞUBAT 2021

Semiha KOŞU, an M.Sc. student of ITU Graduate School 705181014 successfully defended the thesis entitled "COOPERATIVE VEHICULAR COMMUNICATION SYSTEMS WITH PHYSICAL LAYER SECURITY AND NOMA TECHNIQUES", which she prepared after fulfilling the requirements specified in the associated legislations, before the jury whose signatures are below.

Thesis Advisor :	**Prof. Dr. Lütfiye DURAK ATA** Istanbul Technical University	.....
Co-advisor :	**Dr. Serdar Özgür ATA** TÜBİTAK/BİLGEM	.....
Jury Members :	**Prof. Dr. İbrahim ALTUNBAŞ** Istanbul Technical University	.....
	Prof. Dr. Serhat ERKÜÇÜK Kadir Has University	.....
	Asst. Prof. Semiha TEDİK BAŞARAN Istanbul Technical University	.....

Date of Submission : **22 January 2021**
Date of Defense : **10 February 2021**

To my Venus,

FOREWORD

In this thesis, I would like to extend my sincere thanks to my dear advisors Prof. Dr. Lütfiye DURAK ATA and Dr. Serdar Özgür ATA, for invaluable insight into my studies. They extended a great amount of assistance for supporting my studies during my master's degree. I would like to thank them for encouraging my research and for allowing me to grow as a research scientist.

Besides my advisors, I would also like to thank my committee members, Prof. Dr. İbrahim ALTUNBAŞ, Prof. Dr. Serhat ERKÜÇÜK and Asst. Prof. Semiha TEDİK BAŞARAN for their insightful comments and encouragement.

I also had great pleasure of working with Mohammadreza BABAEİ. He provided me with encouragement and patience throughout the duration of my master studies. His point of view helped me to discover my success. I would like to thank my friend and soulmate Ebru ÇAKMAKÇIER. Her companionship increased my confidence to believe in myself.

Besides that, I would like to express my gratitude to my family for encouraging me to educate myself and all the unconditional support during my studies. A special thank you to my little brother, Barış KOŞU. I simply couldn't have done this without him.

This success would not have been possible without all of you.

This work was supported by the Research Fund of Istanbul Technical University. Project Number: MYL-2019-42491. This work is supported in part by Istanbul Technical University (ITU) Vodafone Future Lab under Project No. ITUVF20190901P02.

February 2021

Semiha KOŞU
(Electrical and Electronics Eng.)

TABLE OF CONTENTS

Page

ABBREVIATIONS

AF	**:** Amplify-and-forward
AWGN	**:** Additive white Gaussian noise
BEP	**:** Bit error probability
BS	**:** Base station
CDF	**:** Cumulative distribution function
CDMA	**:** Code division multiple access
CSI	**:** Channel state information
DF	**:** Decode-and-forward
DH	**:** Dual-hop
DHSS	**:** Direct-sequence spread spectrum
E	**:** Eavesdropper
e2e	**:** End-to-end
EGC	**:** Equal gain combining
FDMA	**:** Frequency division multiple access
FHSS	**:** Frequency-hoping spread spectrum
HD	**:** Half-duplex
i.i.d	**:** Independent and identically distributed
LoS	**:** Line-of-sight
MIMO	**:** Multiple-input multiple-output
MRC	**:** Maximum ratio combining
nLoS	**:** Non-line of sight
NOMA	**:** Non-orthogonal multiple access
OMA	**:** Orthogonal multiple access
OP	**:** Outage probability
OSI	**:** Open system interconnection
PDF	**:** Probability density function
PEP	**:** Pairwise error probability
PLS	**:** Physical layer security
PPSC	**:** Probability of positive secrecy capacity
S, R, D	**:** Source, relay, destination
SC	**:** Selection combining
SEP	**:** Symbol error probability
SIC	**:** Successive interference cancellation
SINR	**:** Signal-to-interference and noise ratio
SISO	**:** Single-input single-output
SNR	**:** Signal-to-noise ratio
SOP	**:** Secrecy outage probability
TAS	**:** Transmit antenna selection
TDMA	**:** Time division multiple access
URRLC	**:** Ultra-reliable and low-latency communication
V2V	**:** Vehicle-to-vehicle
V2X	**:** Vehicle-to-everything

SYMBOLS

$\delta(\cdot)$	: Dirac function
B_c	: Coherence bandwidth
T_c	: Coherence time
B_s	: Signal bandwidth
T_s	: Signal duration
σ_τ	: Delay spread
B_D	: Doppler spread bandwidth
$\bar{\gamma}$	: Average received SNR
σ^2	: Variance
n	: AWGN
$E[\cdot]$	: Expectation operator
$K_v(\cdot)$	: $v-$th order modified Bessel function of the second kind
$\Gamma(\cdot)$	: Gamma function
$\lvert\cdot\rvert$	: Absolute value
$F_\cdot(\cdot)$	: Cumulative distribution function
$p_\cdot(\cdot)$	: Probability density function
$Pr\{\cdot\}$	: Probability operator
$\lvert\cdot\rvert$	: Absolute value
$\ln(\cdot)$	: Natural logarithm
$\log_2(\cdot)$	: Logarithmic function
$Q(\cdot)$	: Gauss function
$W_{\cdot,\cdot}(\cdot)$	: Whittaker function
$G_{p,q}^{m,n}\left(\cdot\middle\vert\begin{matrix}a_p\\b_q\end{matrix}\right)$	: Meijer's G function
$G_{p,q:p_1,q_1:p_2,q_2}^{m,n:m_1,n_1:m_2,n_2}\left(\cdot,\cdot\middle\vert\cdot\middle\vert\cdot\middle\vert\cdot\right)$	: Extended generalized bi-variate Meijer's G function

LIST OF FIGURES

Page

COOPERATIVE VEHICULAR COMMUNICATION SYSTEMS WITH PHYSICAL LAYER SECURITY AND NOMA TECHNIQUES

SUMMARY

In recent years, with mobile communication systems development, higher bandwidths and higher data rates are required for individual users. Moreover, in the next-generation wireless communications (5G+), with the emergence of smart cities, many autonomous vehicles and infrastructures are expected to connect. In addition to these numerous connections, it must provide ultra-reliable and low-latency communication (URLLC), which is also necessary for next-generation wireless communications. There are studies examining system performance in vehicle-to-vehicle (V2V) and vehicle-to-everything (V2X) communication systems in the literature. The inter-vehicle environment requires lower antenna heights, cost, and hardware complexities due to the high mobility of vehicles compared to other traditional mobile environments. Also, fading environments in inter-vehicle systems are different from those of stationary users in the literature. Besides, this inter-vehicle fading medium is assumed to be the product of channels in the conventional fading medium and is called the cascade channel model. Therefore, the cascade channel model has an adverse effect on overall system performance. However, some techniques have been studied in the literature which improves V2V system performance.

Cooperative communications and receive diversity techniques are considered as a potential solution for inter-vehicle communication systems. When vehicles are not close enough to each other, the signal may be transmitted over relay nodes, increasing the source coverage area enabling cooperative communications. On the other hand, multiple antenna systems are used to combine signals in the receiver to increase the reliability of the system. The diversity technique at the receiver, which reaches the optimum result by maximizing the received signal-to-noise ratio (SNR), is considered to be the maximum ratio combining (MRC) technique that corresponds to the sum of all SNR values received at the destination. Thus, system performance is improved compared to the use of a single antenna, and the coverage area of the source node is increased with the help of a relay. Also, the relay can use different transmission protocols while transmitting the information of the source. In the decode-and-forward (DF) relaying protocol, the transmitted signal is decoded in the relay first, and then an estimated version of symbol is transmitted to the target node. In the amplify-and-forward (AF) relaying protocol, the signal received on the relay is amplified and then transmitted to the destination. Unlike DF relaying protocol, the noise component is also amplified and sent to the destination in this transmission technique as a disadvantage.

In this thesis, a comparison of DF and AF relaying protocols are studied, assuming that all nodes are mobile in the system. Also, the channels between all vehicle nodes are designated as cascade Rayleigh fading. It is also assumed that the relay is placed co-linearly and with equal distance between source and destination. Moreover, the

relay is equipped with a multi-antenna and applies the MRC technique. Results are provided in terms of bit error probability (BEP) versus SNR values. Accordingly, the increasing number of antennas have improved system performance for both AF and DF relaying protocols. As a result, it is shown that the obtained mathematical expressions are consistent with the Monte-Carlo simulation results.

With the tremendous increase in mobile devices in recent years, the continuous broadcast feature of mobile nodes has become a fundamental problem for ensuring security in the system. Therefore, information can become available even to illegitimate listeners. In the open system interconnection (OSI) model, as the physical layer is critical, it is crucial to provide security and transmitting secure information to other layers. Jammer and eavesdropper are the two main types of physical layer attacks studied in the literature. In jamming attacks, the jammer deliberately generates a noise, causing the received signal to be distorted at the destination. However, in eavesdropping attacks, the eavesdropper intercepts the confidential information transmitted to the destination. In all types of attacks, the secrecy capacity of the general system decreases. However, physical layer security (PLS) techniques focusing on increasing system security performance are studied in the literature. For instance, a secret key generation is a PLS technique that increases system security by using the randomness of channels. In this method, the secret key is generated based on the channel state information (CSI) between the legitimate users. Therefore, the data is kept confidential since the illegal user fails to predict the key, even empowering them with high power.

In this thesis, the eavesdropper is equipped with multiple antennas for a realistic scenario and applies the MRC technique. Moreover, the eavesdropper receives the broadcasted information from both source and relay in the proposed vehicular communication system. The channel models between all mobile nodes are assumed as the cascade Rayleigh fading channel. The secrecy capacity in this system is calculated by subtracting the eavesdropper's capacity from the destination node's capacity. As an evaluation criterion, the secrecy outage probability (SOP) is calculated first. SOP gives the expression when the secrecy capacity falls below a particular threshold value. Moreover, the probability of positive secrecy capacity (PPSC) means that the instantaneous secrecy capacity is always greater than zero is examined. For system performance, it is observed that when the number of receiver antennas of the eavesdropper increases, SOP increases, and PPSC decreases. Finally, the theoretical analyses of SOP and PPSC are verified by Monte-Carlo simulations.

In wireless communication networks, several multiple access methods are drawing attention, such as frequency division multiple access (FDMA), time division multiple access (TDMA), and code division multiple access (CDMA). These orthogonal multiple access (OMA) techniques share the same resource and allow multiple users to work simultaneously in a limited spectrum based on frequency, time, or code. In other words, mobile users can access a limited number of the spectrum simultaneously in these techniques. However, spectrum scarcity is encountered in next-generation wireless networks due to users' need for high data rates and limited resources. At this point, the non-orthogonal multiple access (NOMA) technique could be a promising technology for future wireless networks in terms of providing high spectral efficiency and ensuring fairness between users. The basic concept of NOMA is to allocate different power to users and enable them to work on the same resource block

(frequency, time, or code). Besides, NOMA can be classified into two categories, power-domain and code-domain. In power-domain NOMA, the signals of current users are superimposed at the base station (BS) and broadcasted towards the users to decode their signals. The transmitted signal is decoded at the users using the successive interference cancellation (SIC) method, starting from the strong user with better channel quality conditions. Unlike traditional OMA techniques, weak users with poorer channel quality are allocated more transmission power in NOMA, while stronger users with better channel quality are allocated less transmission power. This power allocation can considerably compensate for the trade-off between the quality of service of the system and user fairness.

In this thesis, the cooperative power-domain downlink NOMA system is studied. The BS communicates with two vehicles via the relay node and operates in half-duplex (HD) mode. Also, relay transmits the signal of the source to the users by applying the AF relaying protocol. Since both relay and users have high mobility, the channel corresponding to link BS and relay is subjected to Rayleigh fading. In contrast, the channels between relay and users are considered as double Rayleigh fading. Since transmitted signals of each user are superimposed, the SIC method helps to decode these signals. It is assumed that the signal of weak user is correctly decoded on the strong user's channel. In other words, the SIC technique is performed perfectly. Additionally, system performance is evaluated in terms of outage probability and ergodic capacity. In both analyzes, the results are provided using different system parameters (power allocation, distance and transmission power of the BS) for the users. Besides, the overall system performance is also taken into account. Finally, the numerical results are consistent with the Monte-Carlo simulation results.

FİZİKSEL KATMAN GÜVENLİĞİ VE NOMA TEKNİKLERİ İLE İŞBİRLİKLİKLİ ARAÇLAR ARASI İLETİŞİM SİSTEMLERİ

ÖZET

Son yıllarda, mobil iletişim sistemlerinin gelişmesiyle birlikte, bireysel kullanıcılar için daha yüksek bant genişlikleri ve daha yüksek veri hızları gerektirmektedir. Öte yandan, yeni nesil kablosuz iletişimde (5G+), akıllı şehirlerin de ortaya çıkmasıyla birlikte çok sayıda otonom araç ve altyapının birbirine bağlaması beklenmektedir. Bu sayısız bağlantının yanı sıra, yeni nesil kablosuz iletişimin de gerekliliği olan, ultra güvenilir ve düşük gecikmeli iletişim (URLLC) sağlamalıdır. Literatürde araçtan araca (V2V) ve araçtan her şeye (V2X) iletişim sistemlerinde, sistem performansını inceleyen çalışmalar bulunmaktadır. Araçlar arası ortamlar, diğer geleneksel mobil ortamlara kıyasla, araçların yüksek hareket kabiliyeti nedeniyle daha düşük anten yükseklikleri, maliyet ve donanım karmaşıklıkları gerektirir. Dahası, araçlar arası sistemlerdeki sönümleme ortamları, literatürdeki sabit kullanıcıların sönümleme ortamlarından farklıdır. Ayrıca, bu araçlar arası sönümleme ortamı, geleneksel sönümleme ortamındaki kanalların çarpımı olarak varsayılmış olup kaskat kanal modeli adı verilmiştir. Bu nedenle, kaskat kanal modelinin genel sistem performansı üzerinde olumsuz bir etkisi vardır. Bununla birlikte, literatürde V2V sistem performansını iyileştirmek için bazı teknikler kullanılmıştır.

İşbirliğine dayalı iletişim ve alıcıda çeşitleme teknikleri, araçlar arası iletişim sistemleri için potansiyel bir çözüm olarak kabul edilir. İşbirlikli iletişimde araçlar birbirine yeterince yakın olmadığında, kaynaktan iletilen işaretin kapsama alanını artırmak için sinyal röle düğümleri üzerinden iletilir. Öte yandan, kullanıcılara yönelik veri hızlarını artırmak için, çoklu anten sistemleri alıcıdaki sinyalleri birleştirmek için kullanılır. Alınan işaret-gürültü oranını (SNR) maksimize ederek optimum sonuca ulaştıran alıcıda çeşitleme tekniği, hedefte alınan tüm SNR'ların toplamına karşılık gelen maksimum oranlı birleştirme (MRC) tekniği olarak kabul edilir. Böylelikle tek anten kullanımına göre sistem performansı iyileştirilmiş ve röle yardımı ile kaynak düğümün kapsama alanı artırılmıştır. Ayrıca röle, kaynağın bilgisini iletirken farklı aktarma tekniklerini kullanabilir. Çöz-ve-aktar (DF) tekniğinde, gönderilen işaret ilk önce rölede çözülür ve ardından hedef düğüme iletilir. Yükselt-ve-ilet (AF) aktarma tekniğinde ise rölede alınan işaret yükseltilerek, ardından hedefe iletilir. Ayrıca, bu iletim tekniğinde dezavantaj olarak, kaynaktan alınan işaret çözülmediğinden, gürültü bileşeni de güçlendirilerek hedefe gönderilir.

Bu tezde, tüm sistem düğümlerinin hareketli olduğu varsayılarak, DF ve AF röle iletim stratejilerinin bir karşılaştırması incelenmiştir. Ayrıca, tüm araç bağlantıları arasındaki kanallar, kaskat Rayleigh olarak belirlenmiştir. Buna ek olarak röle, kaynak ve hedef arasına eşit mesefade ve doğrusal olarak yerleştirildiği varsayılmıştır. Ayrıca, röle çoklu anten sistemi ile donatılmıştır ve MRC tekniğini uygulamaktadır. Sonuçlar, artan SNR değerlerine göre bit hata olasılığı (BEP) cinsinden hesaplanmıştır. Buna göre artan anten sayısı, hem AF hem de DF aktarma stratejileri için sistem

performansını iyileştirmiştir. Sonuç olarak, elde eldilen matematiksel ifadelerin Monte-Carlo benzetim sonuçlarıyla tutarlı olduğu da gösterilmiştir.

Son yıllarda mobil cihazların sayısının muazzam artışıyla birlikte, mobil düğümlerin sürekli yayın yapma özelliği sistemde güvenliğin sağlanması için önemli bir sorun haline gelmiştir. Bu nedenle, bilgiler gizli dinleyiciler için bile kullanılabilir hale gelebilir. Açık sistem ara bağlamı (OSI) modelinde, fiziksel katman ilk sırada yer aldığından dolayı burada güvenliğin sağlanması ve diğer katmanlara güvenli bilginin iletilmesi açısından önemlidir. İşaret karıştırıcı ve gizli dinleyici, literatürde araştırılan iki ana fiziksel katman saldırı tipidir. İşaret karıştırıcı saldırılarında, sinyal bozucu kasıtlı olarak bir gürültü üretir ve bu da hedefte alınan işaretin bozulmasına neden olur. Ancak, gizli dinleme saldırılarında, gizli dinleyici, hedefe iletilen gizli bilgileri yakalar. Tüm saldırı türlerinde ise genel sistemin gizlilik kapasitesi azalır. Bu arada, sistemsel güvenlik performansı artırmaya odaklanan fiziksel katman güvenliği (PLS) teknikleri literatürde çalışılmaktadır. Örnek olarak, gizli anahtar üretimi, bir PLS tekniğidir ve kanalların rastgeleliğini kullanarak sistem güvenliğini arttırmaktadır. Bu yöntemde, yasal olmayan kullanıcılar arasındaki kanal durum bilgisine dayalı olarak bir gizli anahtar üretilir. Yasal olmayan kullanıcı anahtarı tahmin edemediği için yüksek güç kullanarak iletilen işarete erişmeye çalışsa bile veriler gizli tutulur.

Bu tezde, gerçekçi bir senaryo oluşturulmak istendiğinden, çoklu antenlerle donatılmış gizli dinleyicinin, alıcıda çeşitleme yöntemi olan MRC tekniğini uygulayarak araçlar arası iletişim sisteminde hem kaynaktan hem de röleden gönderilen bilgileri dinlediği varsayılmıştır. Tüm mobil düğümler arasındaki kanal modeli ise kaskat Rayleigh sönümlemeli kanal olarak belirlenmiştir. Bu sistemdeki gizlilik kapasitesi, gizli dinleyicinin kapasitesinin alıcı düğümün kapasitesinden çıkarılarak hesaplanmaktadır. Değerlendirme kriteri olarak öncelikle gizlilik kesinti olasılığı (SOP) hesaplanmıştır. SOP, sistem gizlilik kapasitesinin belli bir eşik değerinin altına düştüğü zamanki ifadesini vermektedir. Ayrıca anlık gizlilik kapasitesinin her zaman sıfırdan büyük olduğu anlamına gelen pozitif gizlilik kapasitesi (PPSC) olasılığı hesaplanmıştır. Sistem performansı incelendiğinde, gizli dinleyicin alıcı anten sayısı arttığında SOP'un arttığı ve PPSC'nin ise azaldığı gözlemlenmiştir. Son olarak teorik analizleri Monte-Carlo benzetimleri ile doğrulanmıştır.

Kablosuz iletişim ağlarında, frekans bölmeli çoklu erişim (FDMA), zaman bölmeli çoklu erişim (TDMA) ve kod bölmeli çoklu erişim (CDMA) gibi birkaç çoklu erişim yöntemi dikkat çekmektedir. Bu dikgen çoklu erişim (OMA) teknikleri aynı kaynağı paylaşırlar ve birden fazla kullanıcının frekans, zaman veya koda göre sınırlı bir spektrumda aynı anda çalışmasına izin verirler. Diğer bir deyişle, bu tekniklerde, mobil kullanıcılar aynı anda sınırlı miktardaki frekans bandına erişebilirler. Bununla birlikte, kullanıcıların yüksek veri hızlarına ulaşması ve sınırlı sayıda kaynak kullanımı nedeniyle, yeni nesil kablosuz ağlarda spektrum yoksunluğu ile karşı karşıya kalınmaktadır. Bu noktada, dikgen olmayan çoklu erişim (NOMA) tekniği, yüksek spektral verimlilik sağlaması ve kullanıcılar arası adaleti sağlaması açısından gelecekteki kablosuz ağlar için umut verici bir teknoloji olabilir. NOMA'nın temel konsepti, kullanıcılara farklı güç tahsis ederek aynı kaynak bloğunda (frekans, zaman ya da kod) çalışmalarını sağlamaktır. Bunun yanı sıra, NOMA güç tabanlı ve kod tabanlı olarak iki kategoride sınıflandırılabilir. Güç tabanlı sınıflandırmada, mevcut kullanıcının sinyali, verici tarafında üst üste bindirilerek ve hedef kullanıcının bu işareti çözmesi için yayınlanır. Gönderilen sinyal, daha iyi kanal kalitesi koşullarına

sahip olan güçlü kullanıcıdan başlayarak, ardışık girişim önleme (SIC) yöntemi kullanarak alıcı düğümünde çözülür. Geleneksel OMA tekniklerinden farklı olarak NOMA'da, daha kötü kanal kalitesine sahip zayıf kullanıcılara daha az iletim gücü tahsis edilirken, daha iyi kanal kalitesine sahip güçlü kullanıcılara daha fazla iletim gücü tahsis edilir. Bu güç tahsisi, sistemin hizmet kalitesi ile kullanıcılar arasındaki adaleti önemli ölçüde telafi etmeye çalışır.

Bu tezde, işbirlikli ve güç tabanlı aşağı bağlantılı NOMA sistemi incelenmiştir. Baz istasyonu (BS), röle (R) aracı vasıtasıyla hedef düğümdeki iki araç ile iletişim kurar ve yarı çift yönlü (HD) modda çalışır. Ayrıca, R, AF iletim tekniğini uygulayarak kaynağın sinyalini hedefe iletir. Hem R hem de kullanıcılar yüksek mobiliteye sahip olduğundan, BS $\rightarrow$ R arasına karşılık gelen kanal Rayleigh dağılımına maruz kalırken, R ile hedef kullanıcılar arasındaki kanal çift Rayleigh dağılımı olarak kabul edilmiştir. Her kullanıcı için iletilen sinyaller üst üste bindirildiğinden, SIC yöntemi bu sinyallerin hedef kullanıcılarda çözülmesine yardımcı olur. Burada, zayıf kullanıcının sinyalinin güçlü kullanıcının kanalında doğru bir şekilde çözüldüğü varsayılmıştır. Diğer bir deyişle SIC tekniği kusursuz bir şekilde gerçekleştirilmiştir. Ayrıca, sistem performansı, tam kesinti olasılığı ve ergodik kapasite açısından değerlendirilmiştir. Her iki analizde de sonuçlar, kullanıcılar için farklı sistem parametreleri (güç tahsisi, mesafe ve BS'nin iletim gücü) kullanılarak değerlendirilmiştir. Ayrıca genel sistem performansı da dikkate alınmıştır. Son olarak, sayısal sonuçlar Monte-Carlo benzetim sonuçları ile uyumluluk göstermiştir.

1. INTRODUCTION

Every day, the need for communication is continuously increasing since more and more devices are connected. Meanwhile, with the development of wireless communication technologies, the need for high data rate and reliability of the wireless communication systems is increasing, which results in a challenge for providing the solutions for the available spectrum. Moreover, to create smart infrastructures, communication between fixed nodes and autonomous vehicles and the base station is of absolute importance. Therefore, in this thesis, the performance of cooperative communication systems are investigated where the channels are exposed to cascade Rayleigh fading. Besides, the theoretical expression of the secrecy capacity of a cooperative system is derived in the physical layer perspective for the possibilities of security problems in the system. The design and performance of the next-generation communication system based on cooperative communication and non-orthogonal multiple access (NOMA) techniques is investigated. By applying NOMA technique in the communication system, the efficient use of spectrum for the next-generation wireless communication systems can be increased even more, and it is aimed to contribute to the existing studies in this field.

1.1 Literature Review

Vehicular communication provides a promising solution for next-generation wireless networks. This type of communication is applied to regulate traffic and increase road safety since it is assumed as a part of the intelligent transportation system in the near future. Meanwhile, the type of fading characteristic in a mobile environment with high mobility is investigated in the literature [1–8].

Various studies in the literature investigate the performance of relay-assisted vehicle-to-vehicle (V2V) communication systems [1–5]. The outage performance of a dual-hop (DH) V2V system with the best relay selection applying the amplify-and-forward (AF) relaying protocol is studied in [1] where the channels are exposed to Rayleigh fading. In [2], the average symbol error probability (SEP)

and the outage probability (OP) analyses are derived for the interference-limited cooperative communication systems when the relay applies decode-and-forward (DF) relaying protocol, and the links are exposed to the double Nakagami-*m* fading channel. Moreover, the authors in [3] are studied a multi-hop DF relaying V2V communication system. Furthermore, a tight upper bound pairwise error probability (PEP) expression is derived where the links are exposed to the frequency-selective Rician channel. The outage performance analysis of the upper and lower bound expressions of a two-way V2V communication system are calculated in [4]. Additionally, the relay applies antenna selection over double Rayleigh channels. An approximated OP analysis is calculated for the multi-hop vehicle communication systems in [5]. Here, the relays apply DF and AF relaying protocol to transmit the source signal to the destination using a maximum ratio combining (MRC) scheme. The system performance considering a different number of relay over the cascade mixed channel model (RayleighxRice and double Rayleigh) is investigated in [6] where the relays apply fixed-gain AF relaying protocol. Moreover, the performance is evaluated considering the level-crossing rate average duration. The authors in [7] investigate the BER performance analysis of both DH DF/AF relaying protocols. Moreover, comparison results are also provided between these relaying protocols where the links are exposed to double Rayleigh fading channels. In [8], using bidirectional AF relaying over cascaded Nakagami-*m* channels, the performance is evaluated using moment generating function and higher-order moments of signal-to-noise ratio (SNR). Furthermore, the theoretical expressions of ergodic capacity and average symbol error probability of the proposed system are obtained.

Moreover, the secrecy capacity of the V2V wireless communication system and the physical layer security technique are also investigated in the literature. Secrecy issue is essential since the jammer and eavesdropper (E) can intercept or overhear the confidential data, which then can cause a disaster or accident for the autonomous vehicles or other events. Hence, there are still challenges and open issues about privacy issues.

Secrecy performance of a multi-antenna system in the presence of the direct transmission between a source (S) and a destination (D) is investigated in [9]. Moreover, S, D, and E apply TAS and MRC, respectively. Furthermore, the system

is analyzed concerning secrecy outage probability (SOP), asymptotic SOP, and the probability of positive secrecy capacity (PPSC) over $\alpha - \mu$ fading channels. In [10], the secrecy performance of the cooperative DF relaying is studied according to whether MRC is performed in D and E or not. Moreover, the secrecy capacity of the proposed cooperative system is investigated considering the absence/presence of a direct link between S→D where DF relaying protocol is applied in the absence of a direct link. Additionally, the performance of both cases is compared with each other [10]. On the other hand, in [11], SOP performances of a cooperative relay system applying the DF relaying protocol is investigated considering Rayleigh fading channels.

The secrecy performance of cascading channels is considered in [12–14]. The average secrecy capacity, SOP, and PPSC analysis over double Nakagami- m fading channel is investigated in [12]. Moreover, the authors in [13] extent the studied model in [12]. Here, the system performance is investigated where the links are exposed to N^*Nakagami-m fading. Results are obtained for a different number of cascade channels [13]. Additionally, a similar work is studied in [14] for cascade $\alpha - \mu$ channels. Blocking capacity for the best and closest eavesdroppers with many eavesdropper scenarios is calculated for the cascade Fisher-Scedecor channel model in [15] where blocking capacity is considered as a new performance metric. However, there are very few studies investigating the secrecy performance of cooperative systems in cascade fading channels [16, 17]. In [16], for the hybrid case, where the channels between nodes are modeled with Rayleigh or double Rayleigh fading channel, the SOP and ergodic secrecy capacity of the system is calculated by applying the AF relaying protocol in the absence/presence of a direct link between S-D and S-E. On the other hand, SOP analysis is performed for the double Rayleigh fading channel for the case where the best relay is chosen among the multiple DF relaying relays [17].

So far, power-domain downlink NOMA is extensively studied in the literature [18–29]. The performance of power-domain downlink NOMA-based point-to-point system is studied in [18–20]. Bit error rate (BER) performance of two users applying traditional NOMA receivers with an optimal design is studied in [18] under the assumption of in-phase/quadrature-phase imbalance. Moreover, for different fading channel models, BER performance is investigated in [19] for multi-path channels, various modulation schemes, and channel coding rates. Furthermore, achievable sum-rate analysis is

investigated considering 2K users in [20]. Besides, the users are uniformly distributed in a disc and paired into different numbers of clusters where the base station (BS) is located at the center of the disc. Also, analytical expressions are derived considering Rayleigh fading.

In recent works, cooperative NOMA networks have been studied in [21–29] where the effect of NOMA technique on the capacity and reliability of the considered system is investigated. The authors in [21–23] study the performance of cooperative DF relaying protocol in NOMA-based networks. Ergodic capacity and outage probability of a cooperative NOMA-based under perfect successive interference cancellation (SIC) conditions are studied [21]. It is assumed that all channels are exposed to Rayleigh fading, where a pair of near users communicates with BS. Furthermore, in the absence of a direct link between BS and far user, near users act as a relay and transmit the signal to the far user applying DF relaying protocol. Besides, similar to the proposed system model in [21], the authors in [23] investigate BER performance assuming two user network under statistical channel state information (CSI). Additionally, overall outage probability and sum-rate of the proposed system over α-η-κ-μ fading channels is performed in [22].

Power-domain downlink NOMA-based AF relaying networks have also gained attention in the literature [24–29]. Performance of a cooperative AF relaying with both direct and cooperative link transmission is investigated in [24]. Moreover, a selection combining technique at the users for two information symbols for multiple users is applied. Under perfect SIC condition, when the near user helps the far user over Nakagami-m fading channel, its performance is analyzed in terms of outage probability and throughput [29]. In a cooperative multiple user NOMA network, system performance is investigated under perfect SIC condition [27] and imperfect SIC condition [26]. In multiple-input multiple-output (MIMO) networks using AF relaying protocol, the system performance is evaluated in terms of outage probability when the channels are ordered [25].

Additionally, there are some studies considering NOMA based vehicular communications. In [30], critical problems of V2V NOMA networks and solutions of resource allocation and signalling control algorithms with future applications have been presented. Two users point-to-point V2V scheme is studied over double Rayleigh

fading channels [31]. The same system model is also investigated considering double Nakagami-*m* fading channel with optimal power allocation and the probability of successfully decoding [32].

1.2 Contribution of the Thesis

In section 4, a multi-antenna relay assisted vehicular communication system is investigated. The channels between all the nodes are assumed as cascaded Rayleigh fading. A source, relay, and destination nodes are co-linearly distributed in a straight line when there is no direct link between the source and the destination. In this scheme, the relay combines the signal with the MRC technique and forwards the received signal to the destination considering both DF and AF relaying protocols. The comparison of these protocols is also provided in this thesis for the first time in the literature. The theoretical results are obtained in terms of bit error probability and verified by Monte-Carlo simulations.

In section 5, the cooperative V2V communication system in which the source and destination nodes communicate through relay where the direct link is in a deep fade is studied. It is assumed that the relay applies DF relaying protocol. Moreover, a multi-antenna eavesdropper listens to both source and relay transmitted signals and applies the MRC protocol. Since all nodes are in motion, the corresponding channel between all the links undergoes cascaded Rayleigh fading. Moreover, closed-form expressions of SOP and PPSC are obtained. Monte-Carlo simulation results verify theoretical results.

In section 6, the NOMA based cooperative fixed-gain AF relaying network for vehicle communications is proposed, which improves system capacity and increases spectral efficiency. Also, it is assumed that there is no direct transmission between BS and users. The channels between the relay and the users are assumed to be double Rayleigh fading, which is best suited for the vehicle environment [33]. However, the channel between BS and relay is exposed to Rayleigh fading. To the best of the author's knowledge, no studies have been reported in the literature investigating the cooperative vehicle network over the double Rayleigh fading channel. Moreover, it is assumed that the perfect SIC condition is applied to better diversity ranking than the imperfect SIC scenario [23]. First of all, exact analytical expressions for the user's

signal-to-interference and noise ratio (SINR) values and the outage performance are obtained in closed-form. Second, users and overall system performance are analyzed with the exact ergodic capacity to gain greater insight throughout the paper. System performance is evaluated in terms of transmit power, distance, and power allocation metrics. Monte-Carlo simulations verify the derived theoretical results.

List of the conference and journal publications presenting the original contributions of this thesis to the wireless communication literature is given below:

- S. Koşu, S. Ö. Ata and L. Durak-Ata 2019. On the Error Performance of Relay-Assisted Vehicular Communication Systems, *IEEE Microwave Theory and Techniques in Wireless Communications (MTTW)*, Riga, Latvia, 2019, pp. 68-71, doi: 10.1109/MTTW.2019.8897226.

- S. Koşu, S. Ö. Ata and L. Durak-Ata 2019. Physical Layer Security Analysis of Cooperative Mobile Communication Systems with Eavesdropper Employing MRC, *28th Signal Processing and Communications Applications Conference (SIU)*, Gaziantep, Turkey, 2020, pp. 1-4, doi: 10.1109/SIU49456.2020.9302397.

- S. Koşu, S. Ö. Ata and L. Durak-Ata 2021. NOMA-based Cooperative V2V Communication Systems Employing Fixed-Gain AF Relaying has been preparing for submission.

2. WIRELESS COMMUNICATION CHANNELS AND FADING MODELS

In wireless communication, the transmitted signal from the transmitter is passed through a medium called a channel, following different paths. This signal can be reflected or scattered from other objects in the medium such as buildings, cars, etc., and this effect is described as "shadowing". Thus, the destination receives the sum of the signal, which includes amplitudes and phase changes and delay of the originally transmitted signal. Additionally, this transmission can cause rapid and large magnitude and phase changes of the signal due to the delay spread. This significant effect of the medium causes distortions in the signal called "multipath fading". This multipath fading can cause inter-symbol interference, and therefore, this effect adversely reduces the quality and reliability of the communication system. Moreover, the other important factor that negatively impacts communication quality is the distance between the transmitter and the receiver nodes expressed as "path loss". These three mentioned parameters are the keys for analyzing wireless communication performances, and their effects can be shown in Fig. 2.1.

Signals passed through the environment are exposed to multipath fading and shadowing. If the transmitted signal directly reaches the receiver, line-of-sight (LoS)

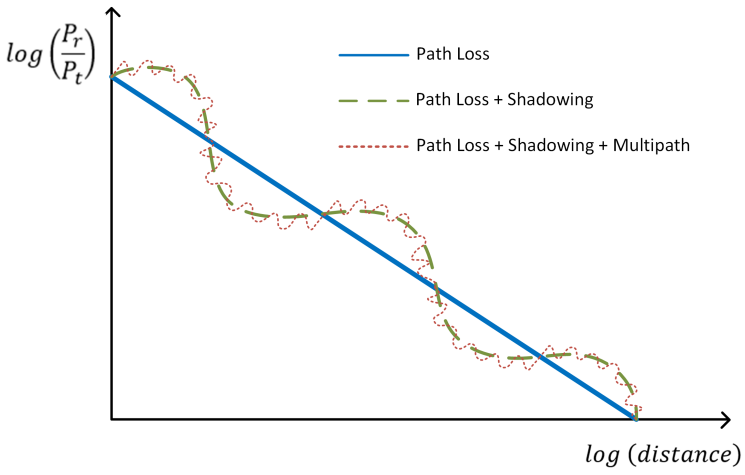

Figure 2.1 : The effect of path loss, shadowing and multipath fading in wireless communications.

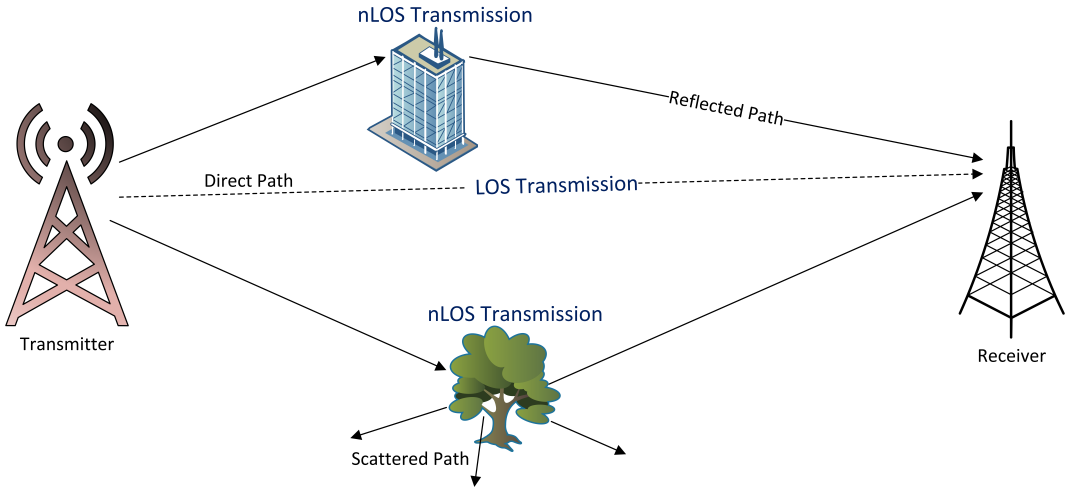

Figure 2.2 : LoS and nLoS transmission schemes performing different multipath.

transmission occurs. However, most of the time, the signal can not be transmitted to the receiver directly due to scattering and reflection effects. In other words, there is the non-LOS (nLoS) transmission between the transmitter and the receiver as in Fig. 2.2.

2.1 Characteristics of Fading Channels

Due to natural character of the channel, the reflected and scattered signals may follow different paths to the receiver with different amplitude and phase fluctuations. In other words, the transmitted signal may vary in time, phase and amplitude until it reaches the receiver as shown in Fig. 2.3.

Then at the receiver, the received signal is the sum of the transmitted signal following multiple paths with different amplitude, phase shift and time delay, which is expressed as

$$r(t) = s(t) * g(t, \tau) = \sum_{i=1}^{L} A_i \, s(t - \tau_i) \, e^{-j\phi_i(t)} \tag{2.1}$$

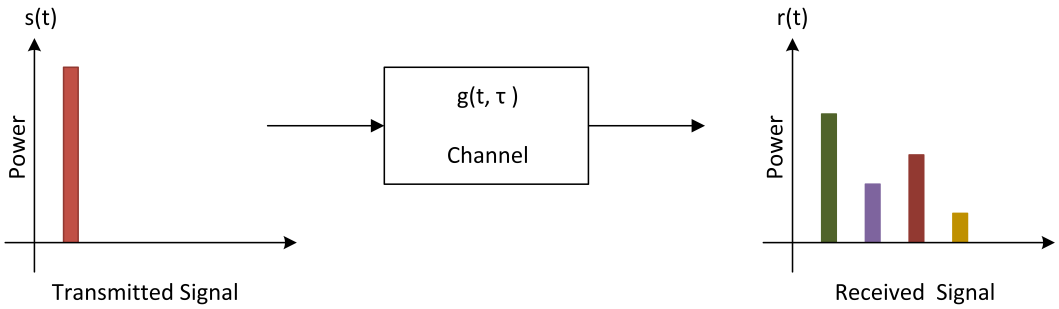

Figure 2.3 : Phase fluctuations of the transmitted signal in time.

where L is the number of paths, τ_i, A_i and ϕ_i are the $i-$th received signal time delay, amplitude and phase shift, respectively for $i = 1, 2, ..., L$. The channel $g(t, \tau)$ is linear time varying and is given as

$$g(t, \tau) = \sum_{i=1}^{L} A_i \, e^{-j\phi_i} \, \delta(\tau - \tau_i). \tag{2.2}$$

In multipath fading, if the fluctuations consist of a long period of time (long term fluctuations), this is called as "large-scale fading" depicted as green dotted lines as in Fig 2.1. On the contrary, short term fluctuations indicate "small-scale fading" represented by the heavily dotted red lines in Fig. 2.1.

Small-scale multipath fading channels can be categorized depending on the relationship between the transmitted signal parameters and the received signal channel parameters. The channel parameters are the Doppler spread, coherence bandwidth/time and delay spread. If the duration of the received signal over the multipath fading channels to the destination expands over time, this effect is defined as "delay spread". Additionally, "Doppler spread" is a measure of the spectral expansion caused by the movement of a mobile node in the multipath fading channel. The received signal at the destination is calculated by considering these effects.

Even though the negative effect of Doppler and delay spread, a signal can be transmitted almost in the same gain and linear phase shift. The bandwidth of the signal passing with less distortion is defined as the "coherence bandwidth (B_c)" and the time interval in which the distortion is distinguishable is denoted as "coherence time (T_c)".

2.1.1 Frequency non-selective and frequency selective fading

In frequency non-selective (flat) fading, coherence bandwidth is larger than the signal bandwidth ($B_c >> B_s$), equivalently delay spread is less than the signal duration ($\sigma_\tau << T_s$). On the contrary, the conditions $B_c < B_s$ or $\sigma_\tau > T_s$ represents frequency selective fading.

2.1.2 Slow and fast fading

Slow fading occurs if the signal duration is considerably less than coherence time ($T_s << T_c$). In this case, signal bandwidth is larger than Doppler spread bandwidth ($B_s >> B_D$). However, for $T_s > T_c$ or $B_s < B_D$ case , fast fading occurs.

2.2 Models for Small-Scale Fading

The most encountered and simplest model for analyzing system performance in wireless communication is considering the system which exposes only to additive white Gaussian noise (AWGN) in which the power spectral density is constant for all frequencies. Therefore, the AWGN channel is an ideal channel model. However, this model is not suitable for characterizing realistic signal transmission in fading channels whose transmission characteristic changes over time, and it is only suitable for describing the behavior of the noise channels. There are several fading models that describe short-term fading behavior, such as Rayleigh fading, $\alpha - \mu$, cascaded fading, etc.

2.2.1 Rayleigh fading channels

In a mobile radio network, the transmitted signal follows different paths until it reaches the receiver. It can only be reflected or scattered from obstacles in the environment. In other words, there is nLOS transmission. Under these conditions, Rayleigh fading is considered as a standard accepted model [34]. The probability density function (PDF) of Rayleigh distribution is given as

$$p_z(z) = \frac{z}{\sigma^2} \exp\left(-\frac{z^2}{2\sigma^2}\right) \tag{2.3}$$

where σ^2 is the power of perpendicular components of Gaussian distribution. Additionally, average channel power is expressed as $\Omega = E[|Z|^2] = 2\sigma^2$ where $E[.]$ is the expectation operator. Fig. 2.4 depicts the Rayleigh distribution with different variance values.

There are also other channel fading models in wireless communication, including Nakagami-n (Rician) fading that analyzes LoS transmission while Nakagami-m considers both LoS and nLoS transmission. Note that the Nakagami-m distribution

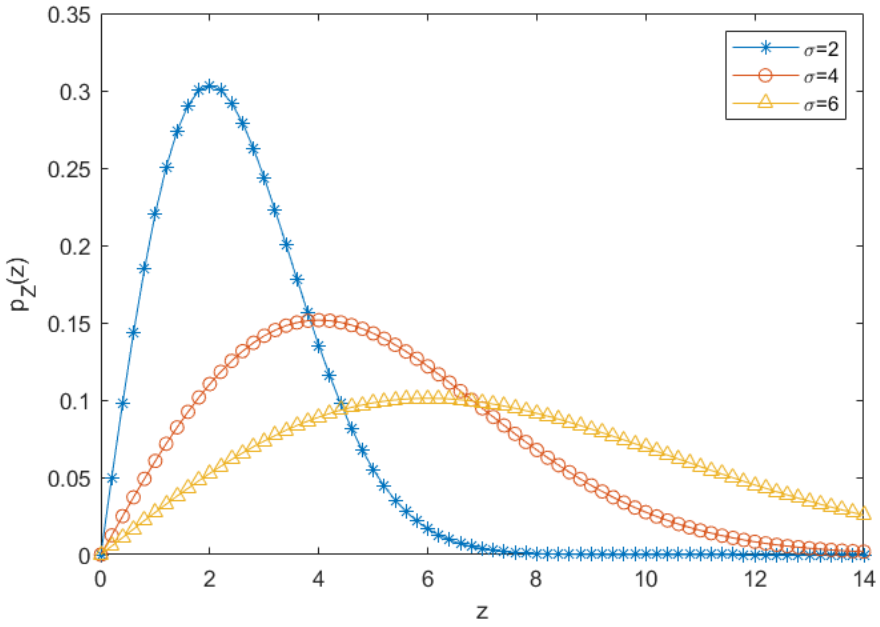

Figure 2.4 : PDF of Rayleigh distribution with respect to different variance parameters.

allows modeling of a wide variety of fading channel environments in which the Rician distribution cannot model dense scattering conditions, and it considers the presence of LoS path between the transmitter and the receiver.

2.2.2 Cascaded fading channels

Unlike classical fading distributions, assumed for the fixed node, different distributions are also provided in the literature for mobile nodes. Therefore, cascaded channel models consider the vehicular fading environment, and they are generally the product of classical distributions. The considered mathematical model of cascaded channel fading is expressed as

$$h = \prod_{i=1}^{N} h_i \tag{2.4}$$

where N indicates number of channels. If $N = 2$ and h_i is Rayleigh distributed random variable, h is considered as double-Rayleigh distributed random variable. Then the PDF and cumulative distribution function (CDF) expressions of the SNR over double Rayleigh fading channels are expressed as [35]

$$p_\gamma(\gamma) = \frac{2}{\bar{\gamma}} \mathrm{K}_0 \left(2\sqrt{\frac{\gamma}{\bar{\gamma}}} \right), \tag{2.5}$$

$$F_\gamma(\gamma) = 1 - 2\sqrt{\frac{\gamma}{\bar{\gamma}}}\,\mathrm{K}_1\left(2\sqrt{\frac{\gamma}{\bar{\gamma}}}\right) \tag{2.6}$$

where $\gamma = |h|^2$ and $K_v(.)$ is the $v-$th order modified Bessel function of the second kind [36]. Additionally, for the general case of N*Rayleigh fading the PDF is given as [37],

$$p_h(x) = \frac{2}{\sqrt{2^N\sigma^2}} G_{0,N}^{N,0}\left((2^N\sigma^2)^{-1}x^2\Big|_{\frac{1}{2},\frac{1}{2},\ldots,\frac{1}{2}}^{-}\right) \tag{2.7}$$

where $G_{p,q}^{m,n}(.|:)$ denotes Meijer's G-function [36, eq. 9.31-1].

2.2.3 Gamma-Gamma distribution

Gamma-Gamma distribution is considered as a model that includes shadowing and fading effects in wireless networks and is mostly used in optical communication systems. Moreover, this distribution is suitable for considering cascade multipath fading channels. The PDF and CDF of the SNR with the Gamma-Gamma distribution are given as [38]

$$p_\gamma(\gamma;k,m,\Omega) = \frac{2(km)^{\frac{k+m}{2}}\gamma^{\frac{k+m}{2}-1}}{\Gamma(m)\Gamma(k)\Omega^{\frac{k+m}{2}}} K_{k-m}\left[2\left(\frac{km}{\Omega}\gamma\right)^{\frac{1}{2}}\right], \tag{2.8}$$

$$F_\gamma(\gamma;k,m,\Omega) = \frac{1}{\Gamma(m)\Gamma(k)} G_{1,3}^{2,1}\left(\frac{km}{\Omega}\gamma\Big|_{k,m,0}^{1}\right) \tag{2.9}$$

respectively where $\Gamma(.)$ is the Gamma function [36], $E[\gamma] = E[|h|^2] = \Omega$. In addition, for the special case of $k = 1$ and $m = 1$, $p_\gamma(\gamma;1,1,\Omega)$ in (2.8) reduces to double-Rayleigh fading as in (2.5) and $F_\gamma(\gamma;1,1,\Omega)$ in (2.9) reduces to (2.6).

In this section, a general view of wireless communications and the characteristic of fading channels are discussed. Additionally, some small-scale fading distributions are also mentioned. In the next chapter, diversity techniques and cooperative systems are provided.

3. COOPERATIVE COMMUNICATION SYSTEMS

In wireless communication, due to the negative impact of the short-term fading to the system performance, outage probability, and the bit error rate of the wireless system becomes worse than the non-fading case, which is only affected by noise. However, the deterious effect of short-term fading can be decreased by applying diversity techniques, which results in better system performances. The diversity techniques can be applied by time, frequency, space, angle, polarization, multipath, and modulation.

In the literature, a typical point-to-point system model is single-input single-output (SISO) shown in Fig. 3.1(a) [39]. In this model, the signal is transmitted at a single angle with no diversity applied. However, different system models exist using multiples antennas which increase reliability and throughput compared to the SISO model where it is denoted as multiple-input multiple-output (MIMO). The illustration of MIMO model is shown in3.1(b). In this model, the multi-antenna enables diversity techniques to be applied on both the transmitter and receiver side. In this way, system performance achieves higher data rates.

Diversity techniques can be basically categorized as receive and transmit diversities. The other methods which increase the system performance is increasing transmitted power and/or antenna size. However, mobile nodes have limited transmit power and

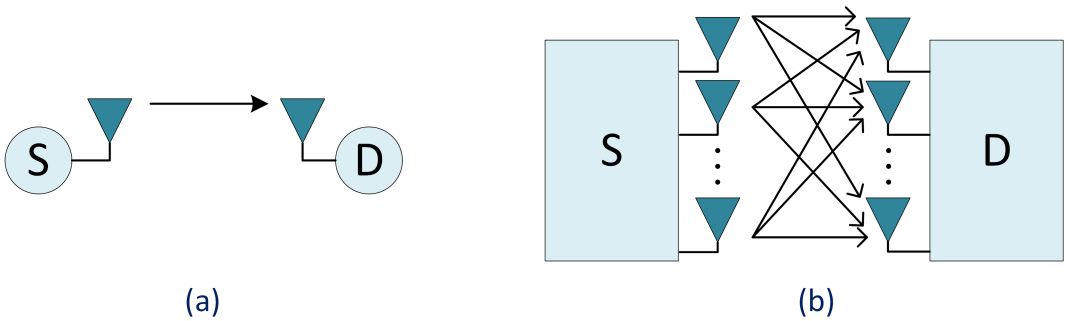

Figure 3.1 : Illustration of SISO and MIMO systems.

small in size. Then, increasing transmit power is not an effective solution for increasing system performance. Therefore, transmit and/or receive diversity should be applied.

3.1 Receive Diversity Combining Techniques

In wireless communication, to employ receiver diversity, the signals coming from independent fading paths are combined to achieve output signal with multiple receive antennas. The concept of the receiver diversity scheme is shown in Fig. 3.2 and the system selects the certain combination of the received signals with gain factors ω_i for $i \in \{1,2,\ldots,L\}$ as in Fig. 3.2. Here, it is assumed that there are L receiving antennas with independent fading channels h_i for $i \in \{1,2,\ldots,L\}$.

The received signal on each branch is expressed as

$$r_i = h_i s + n_i \tag{3.1}$$

where s is the transmitted signal and n_i is the additive white Gaussian noise (AWGN) with single-sided power spectral density of N_o. Furthermore, the received signal-to-noise ratio (SNR) for each branch using (3.1) is calculated as

$$\gamma_i = |h_i|^2 \frac{E_s}{N_o} \tag{3.2}$$

where E_s is the average energy of the transmitted symbol. In the literature, primary receive diversity combining algorithms are selection combining (SC), maximum ratio combining (MRC), and equal gain combining (EGC).

3.1.1 Selection combining

The most straightforward technique of receiver diversity is SC. According to Fig. 3.2, the gain value is given as

$$\omega_i = \begin{cases} 1, & \gamma = \max\{\gamma_i\}_{i=1,2,\ldots,L} \\ 0, & \text{otherwise.} \end{cases} \tag{3.3}$$

Based on (3.3), the system processes only one diversity branch where the combiner chooses the branch with the highest SNR which is expressed as

$$\gamma_{sc} = \max\{\gamma_i\}_{i=1,2,\ldots,L}. \tag{3.4}$$

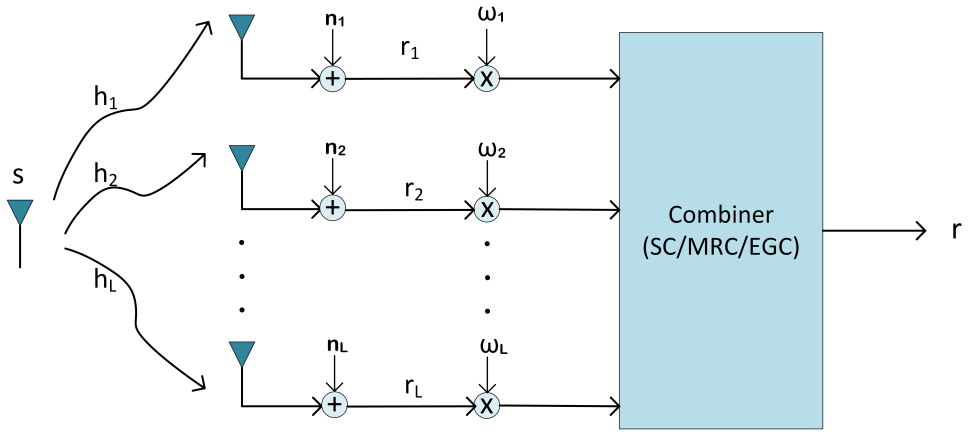

Figure 3.2 : Diversity Combining Techniques Scheme.

The performance of the SC technique is evaluated by calculating cumulative distribution function (CDF) of the received SNR given in (3.4) as

$$F(\gamma_{SC}) = Pr\{\gamma_1 \leq \gamma_{sc}, \gamma_2 \leq \gamma_{sc}, ..., \gamma_L \leq \gamma_{sc}\}. \tag{3.5}$$

Moreover, the CDF of the independently and identically distributed (i.i.d) received SNR is simplified as

$$F(\gamma_{SC}) = [Pr\{\gamma \leq \gamma_{sc}\}]^L. \tag{3.6}$$

3.1.2 Maximum ratio combining

All the received signal on each independent channel is weighted one by one, and the maximum received SNR is obtained at each branch. According to Fig 3.2, the gain factor is set to $\omega_i = h_i^*$ for $i \in \{1,2,\ldots,L\}$ which results maximum received SNR. Therefore, MRC is the optimal combining technique. The combined received signal is

$$r = \sum_{i=1}^{L} r_i\, \omega_i = \sum_{i=1}^{L} |h_i|^2 s + \sum_{i=1}^{L} h_i^* n_i. \tag{3.7}$$

Moreover, the received SNR is expressed as

$$\gamma_{MRC} = \frac{\left(\sum_{i=1}^{L} |h_i|^2\right)^2 E_s}{\sum_{i=1}^{L} |h_i|^2 N_0} = \sum_{i=1}^{L} |h_i|^2 \frac{E_s}{N_0} = \sum_{i=1}^{L} \gamma_i. \tag{3.8}$$

Considering the received SNR as i.i.d. in all branches, the average received SNR is simplified as

$$\bar{\gamma}_{MRC} = L\,\bar{\gamma} \tag{3.9}$$

where $\bar{\gamma} = E[\gamma_i]$. Additionally, MRC technique requires channel state information (CSI) knowledge at each branch to combine signals at the receiver and should be employed simultaneously. Since the received SNR is time-varying on each branch, it requires more complexity than the other combining techniques.

3.1.3 Equal gain combining

In this method, all the received signals at each branch are combined by bringing them to the same phase. Then, the combined received signal is expressed as

$$r = \sum_{i=1}^{L} r_i \, \omega_i = \sum_{i=1}^{L} \rho_i s + \sum_{i=1}^{L} e^{-j\phi_i} n_i \tag{3.10}$$

where $h_i = \rho_i e^{-j\phi_i}$ for $i \in \{1, 2, \ldots, L\}$ and the received SNR is calculated by using (3.10) as

$$\gamma_{EGC} = \frac{\left[\sum_{i=1}^{L} \rho_i\right]^2 E_s}{\sum_{i=1}^{L} N_0} = \frac{\left[\sum_{i=1}^{L} \rho_i\right]^2 E_s}{L N_0}. \tag{3.11}$$

Please note that if all channel gains are equal and deterministic, MRC is equivalent to the EGC.

Performance comparisons of different receive diversity combining techniques are given in Fig. 3.3. As seen from the figure, MRC has the highest SNR gain and is the optimum combining method. However, this method requires more complexity since

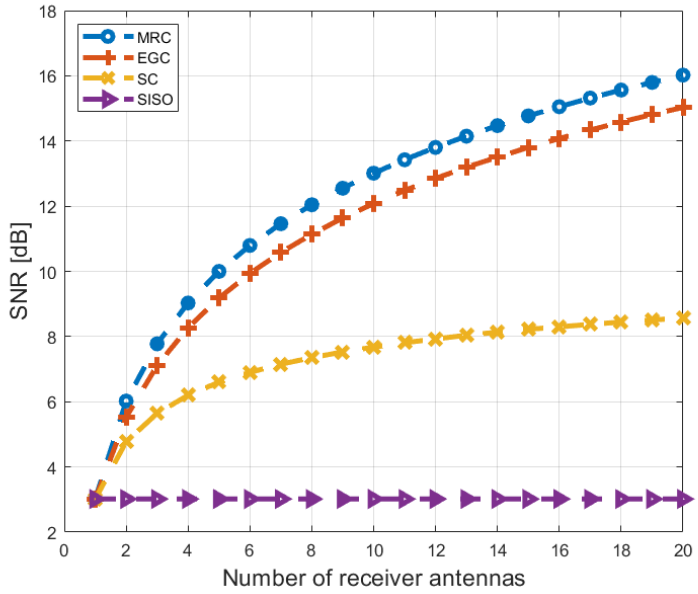

Figure 3.3 : Comparison of SISO, SC, MRC and EGC performances.

the received signal is time-varying, and CSI is required for all diversity branches. EGC performs closely with MRC. Finally, SC is easy to employ and performs significantly better compared to the no diversity case.

3.2 Relaying Protocols

In section 3.1, receive diversity combining techniques that increases the system performance is discussed. On the other hand, these combining techniques may not be appropriate due to the limitations of the mobile environment's cost or size. At this point, cooperative communication will be discussed in this section.

As a result of the studies carried out in recent years in cooperative communication, single antenna mobile units can gain the advantages of MIMO systems. Multiple users with a single antenna in a mobile environment create a virtual MIMO system by sharing their antennas, which provide spatial diversity. Eventually, reliability and efficiency are increased, and fading's deteriorating effect can be reduced in wireless systems.

The signal is transmitted over a statistically independent fading channel to the receiver, which provides spatial diversity and consequently it increases the system performance. Each user who receives the signal and also forwards that information to the next user is called "relay (cooperating unit)". Moreover, different cooperative communication concepts in wireless systems can be shown in Fig 3.4. In Fig 3.4 (a), the source transmits the signal to the destination with the help of relay. Here, the destination is not in the range of the source. In other words, no direct link exists between source

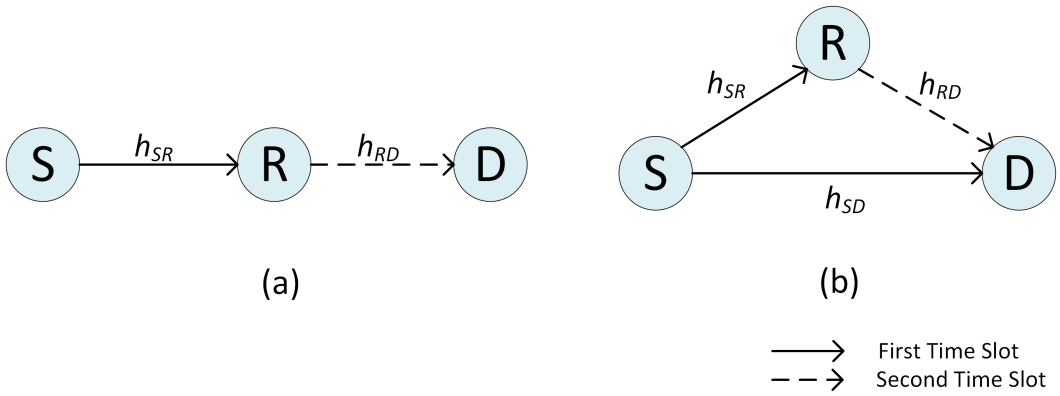

Figure 3.4 : Examples of cooperative communication systems.

and destination. Here, the relay is applied to increase the transmission coverage area. However, in Fig. 3.4 (b), when the destination is in the source's coverage area, both direct and relay link perform transmission. This model provides spatial diversity in which increases system performance. However, these methods cause a 50 percent decrease in spectral efficiency due to two transmission time slot.

The drawback of using cooperative communication results in lower data rates. There are two primary relaying protocols; decode-and-forward (DF) and amplify-and-forward (AF) relaying.

3.2.1 DF relaying

In this technique, relay tries to estimate transmitted symbol from source as in Fig 3.4 (a). Then, in the second time slot, the relay broadcasts the estimated symbol to the destination node. The received signal at relay and destination nodes are given as

$$y_R = \sqrt{P_S}\, h_{SR}\, x + n_R, \tag{3.12}$$

$$y_D = \sqrt{P_R}\, h_{RD}\, \hat{x} + n_D \tag{3.13}$$

respectively, where h_{SR} and h_{RD} represents fading channel coefficients between the links source-relay and relay-destination while P_S and P_R are the transmit power of source and relay nodes, respectively, and $\hat{x}$ is the estimated symbol at the relay. Moreover, n_R and n_D are AWGN at relay and destination, respectively. Realization of this process to get an optimum solution is possible when CSI is available between the nodes.

In this method, if the relay perceives incorrect information, cooperation can have a disruptive effect, which causes the error propagation for the system performance.

3.2.2 AF relaying

In this relaying technique, different from DF relaying protocol, the relay amplifies and forwards the received signal at relay without estimating the symbol to the destination as in Fig 3.4 (a). The received signals at relay and destination are expressed as,

$$y_R = \sqrt{P_S}\, h_{SR}\, x + n_R \tag{3.14}$$

$$y_D = G\, h_{RD}\, y_R + n_D \tag{3.15}$$

where the scaling parameter G is given as

$$G = \sqrt{\frac{P_R}{P_S|h_{SR}|^2 + \sigma_R^2}} \tag{3.16}$$

where σ_R^2 is the noise variance at R. In the AF method, the CSI of all fading channels should be known at the destination. However, in DF relaying protocol, CSI is only known in the related hop.

Please note that, in the AF relaying protocol, the noise is also amplified and forwarded to the destination.

In this section, the cooperative and diversity techniques are discussed. Besides, the advantages and drawbacks of these techniques are also provided. Additionally, for the cooperative systems, DF and AF relaying protocols are reviewed. In the next chapter, the performance cooperative communication in vehicular networks will be discussed.

4. COOPERATIVE COMMUNICATIONS FOR VEHICULAR NETWORKS

In this chapter, we investigate the performance of a dual-hop (DH) vehicle-to-vehicle (V2V) communication system. In this scenario, a multi-antenna relay vehicle employs the maximum ratio combining (MRC) technique to combine the received signals from source to achieve maximum signal-to-noise ratio (SNR) at the receiver side. However, source and destination nodes are equipped with a single antenna. The channels between all the nodes are assumed as double Rayleigh fading, which is suitable for vehicular communications [33]. In this model, the bit error probability (BEP) expressions of both decode-and-forward (DF) and amplify-and-forward (AF) relaying protocols are derived. Moreover, theoretical analysis are verified by the simulation results for both relaying protocols.

4.1 Proposed System Model

In this model, source (S) transmits a signal to the destination (D) via relay (R) node where there is no direct link transmission as illustrated in Fig. 4.1. Besides, all the fading channels between nodes are assumed as double Rayleigh fading. The probability density function (PDF) and cumulative distribution function (CDF) expressions of the instantaneous received SNR for the link R$\rightarrow$D are given as [35]

$$p_{\gamma}(\gamma) = \frac{2}{\bar{\gamma}} \mathrm{K}_0 \left(2\sqrt{\frac{\gamma}{\bar{\gamma}}} \right), \tag{4.1}$$

$$F_{\gamma}(\gamma) = 1 - 2\sqrt{\frac{\gamma}{\bar{\gamma}}} \mathrm{K}_1 \left(2\sqrt{\frac{\gamma}{\bar{\gamma}}} \right) \tag{4.2}$$

where $\bar{\gamma}$ is the expected value of γ and $\mathrm{K}_{\nu}(\cdot)$ is the $\nu-$th order modified Bessel function of the second kind [36]. Here, node S is equipped with a single transmit antenna, and D has a single receive antenna. Moreover, in the absence of the direct link, R is used to increase the source coverage area. Additionally, R is equipped with L antennas which results receive diversity. Finally, the transmission is consist of two time slot as shown in Fig. 4.1. In the first time slot, S broadcast a symbol x to R and the received signal at

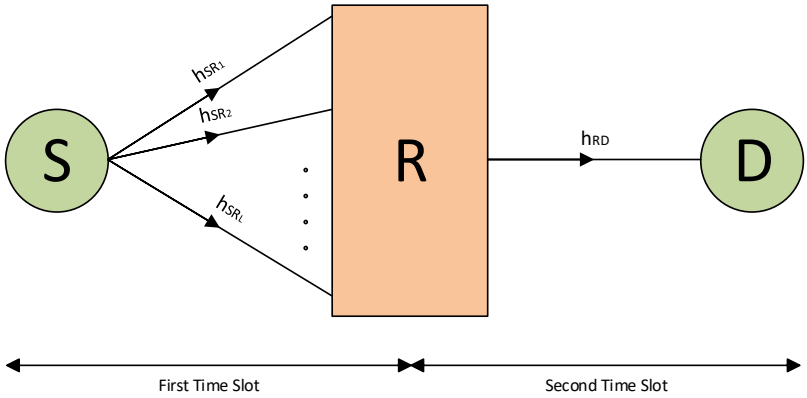

Figure 4.1 : Cooperative V2V communication system model when R applies MRC technique.

each antenna of R for $i \in \{1,2,\ldots,L\}$ is given as

$$y_{R_i} = \sqrt{P_S}\, h_{SR_i} x + n_{R_i} \tag{4.3}$$

where P_S is the average transmitted power of the S. Moreover, h_{SR_i} is the channel fading coefficient for the link S→R and n_{R_i} denotes complex additive Gaussian noise with zero mean and $\sigma^2_{R_i} = N_o$ variance for each antenna at node R. Then, to achieve maximum receive diversity at R, MRC technique is applied and the combined received SNR at R is given as

$$\gamma_R = \sum_{i=1}^{L} \gamma_i \tag{4.4}$$

where $\gamma_i = \frac{P_S}{\sigma^2_{R_i}} |h_{SR_i}|^2$ is the instantaneous received SNR at each antenna of the R. Furthermore, in the second time slot, based on the relaying protocol, the relay forwards a signal to the D.

4.1.1 DF relaying protocol

In DF relaying protocol, the received signal x in the first time slot is estimated at R. In other words, R decodes the signal and then forwards the estimated symbol $\hat{x}$ to the D in the second time slot. Therefore, the received signal at D is written as,

$$y_D^{DF} = \sqrt{P_R}\, h_{RD}\, \hat{x} + n_D \tag{4.5}$$

where P_R is the average transmitted power of the R. Moreover, h_{RD} express the channel fading coefficient for the link R→D and n_D denotes the i.i.d. complex additive Gauissian noise with zero mean and $\sigma^2_D = N_0$ variance at node D. Considering (4.3),

(4.4) and (4.5), the received SNR at nodes R and D are calculated as

$$\gamma_R = \frac{P_S}{\sigma_R^2}|h_{SR}|^2 \qquad \text{and} \qquad \gamma_D = \frac{P_R}{\sigma_D^2}|h_{RD}|^2, \tag{4.6}$$

respectively, where $|h_{SR}|^2 = \sum_{i=1}^{L} |h_{SR_i}|^2$.

4.1.2 AF relaying protocol

In this part, unlike the DF relaying protocol, when AF relaying protocol is applied, the combined received signal at node R is normalized and amplified and then transmitted to D. Meanwhile, the noise term at node R is also transmitted to the D along with the received signal. Therefore, considering (4.3) the received signal at node D in the second time slot is expressed as

$$y_D^{AF} = \sqrt{P_R}\, G\, h_{RD}\, y_R + n_D \tag{4.7}$$

where $y_R = \sum_{i=1}^{L} y_{R_i}$ in (4.3). Furthermore, G is the normalization scaling parameter which is represented as

$$G = \sqrt{\frac{1}{P_S|h_{SR}|^2 + \sigma_R^2}}. \tag{4.8}$$

Then, by substituting (4.8) in (4.7) and after doing mathematical operations, the end-to-end (e2e) SNR at D is expressed as

$$\gamma_{e2e} = \frac{\gamma_R \gamma_D}{\gamma_R + \gamma_D + 1} \tag{4.9}$$

where γ_R and γ_D are given in (4.6). Moreover, we assume a tight upper bound expression instead of using (4.9) which is not analytically tractable. Then, the e2e received SNR is re-expressed as [40]

$$\gamma_{e2e} \leqslant \min(\gamma_R, \gamma_D). \tag{4.10}$$

which is also precise at medium and high SNR. At this point, the CDF of the e2e SNR in (4.10) is represented as [41]

$$F_{\gamma_{e2e}}(\gamma) = F_{\gamma_R}(\gamma) + F_{\gamma_D}(\gamma) - F_{\gamma_R}(\gamma) F_{\gamma_D}(\gamma) \tag{4.11}$$

where $F_{\gamma_x}(\gamma)$ denotes the CDF of the respective nodes where $x \in \{R, D\}$.

4.2 Bit Error Probability Analysis

In wireless communications, the symbol error probability (SEP) is calculated as [34]

$$P_e = a\int_0^{\infty} \mathrm{Q}(\sqrt{2b\gamma}) p_\gamma(\gamma)\mathrm{d}\gamma \tag{4.12}$$

where $p_\gamma(\gamma)$ is the PDF of the received SNR and $\mathrm{Q}(\cdot)$ is the one-dimensional Gauss function [36]. Furthermore, a and b represents the modulation constants for BPSK $a=1$, $b=1$, for coherent BFSK $a=1$, $b=0.5$, for M-PAM $a=2(M-1)/M$, $b=3/(M^2-1)$, for M-QAM $a=4(1-1/\sqrt{M})$, $b=3/2(M-1)$ and for M-PSK $a=2$, $b=\sin^2(\pi/M)$ [42].

However, different from (4.12), SEP also can be calculated as

$$P_e = \frac{a\sqrt{b}}{2\sqrt{\pi}}\int_0^{\infty} \frac{e^{-b\gamma}}{\sqrt{\gamma}} F_\gamma(\gamma)\mathrm{d}\gamma. \tag{4.13}$$

4.2.1 DF relaying protocol

In DF relaying protocol, the overall SEP performance of the considered system should be calculated for each link. Here, overall error performance is upper-bounded as

$$P_e \leq 1-(1-P_e^{SR})(1-P_e^{RD}) \tag{4.14}$$

where P_e^{SR} and P_e^{RD} are the SEP of the links S→R and R→D, respectively. In the first time slot, the SEP of the link S→R can be obtained by using (4.12). Please note that, the PDF of the received SNR over double Rayleigh fading channels can be also represented as a square of Gamma-Gamma distribution [38] is given as

$$p_\gamma(\gamma) = \frac{2(km)^{\frac{k+m}{2}}\gamma^{\frac{k+m}{2}-1}}{\Gamma(k)\Gamma(m)\bar{\gamma}^{\frac{k+m}{2}}} K_{k-m}\left(2\sqrt{\gamma/\bar{\gamma}}\right) \tag{4.15}$$

where $\Gamma(.)$ is the Gamma function. Herein, for double Rayleigh case the parameters should be assigned as $k=1$ and $m=1$. Since R applies the MRC technique, the combined received signal at R in the first time slot as in (4.4) can be denoted as

$$p_{\gamma_R}(\gamma) = \frac{2(k_L m_L)^{\psi}\gamma^{\psi-1}}{\Gamma(k_L)\Gamma(m_L)\bar{\gamma}_R^{\psi}} K_{k_L-m_L}\left(2\sqrt{\frac{k_L m_L}{\bar{\gamma}_R}\gamma}\right) \tag{4.16}$$

where $\psi = \frac{k_L+m_L}{2}$, $k_L = Lk+(L-1)\frac{-0.127-0.95k-0.0058m}{1+0.00124k+0.98m}$, $m_L = Lm$ and $\bar{\gamma}_R = L\bar{\gamma}_i$ for $i \in \{1,2,\ldots,L\}$. Here, we use the fact that the sum of i.i.d squared Gamma-Gamma

random variable in (4.16) is also squared Gamma-Gamma distributed random variable [38], again. At this point, P_e^{SR} in (4.14) is calculated by replacing (4.16) in (4.12) as

$$P_e^{SR} = a\xi \int_0^{\infty} \gamma^{\psi-1} \mathrm{Q}(\sqrt{2b\gamma}) \mathrm{K}_{k_L-m_L}\left(2\sqrt{\beta\gamma}\right) \mathrm{d}\gamma \tag{4.17}$$

where $\beta = \frac{k_L m_L}{\bar{\gamma}_R}$ and $\xi = \frac{2(k_L m_L)^{\psi}}{\Gamma(k_L)\Gamma(m_L)\bar{\gamma}_R^{\psi}}$. Moreover, by substituting [43, eq.2.3-18] and [44, eq.06.27.26.0006.01] in (4.17), we have

$$P_e^{SR} = \frac{a\xi}{4\sqrt{\pi}} \int_0^{\infty} \gamma^{\psi-1} G_{2,3}^{2,1}\left(b\gamma \middle| {}^{1,1}_{0,0.5,1}\right) G_{1,3}^{2,1}\left(\beta\gamma \middle| {}^{1}_{\frac{k_L-m_L}{2}, \frac{m_L-k_L}{2}, 1}\right) \mathrm{d}\gamma \tag{4.18}$$

Here, by using [45, eq.21] the SEP for the link S→R is calculated as

$$P_e^{SR} = \frac{a\xi b^{-\psi}}{4\sqrt{\pi}} G_{4,5}^{3,3}\left(\frac{\beta}{b} \middle| {}^{1,1-\psi,0.5-\psi,-\psi}_{\frac{k_L-m_L}{2}, \frac{m_L-k_L}{2}, -\psi, -\psi, 1}\right). \tag{4.19}$$

In the second time slot of the considered system, to obtain the SEP of the link R→D similar steps are applied. Therefore, by substituting (4.1) into (4.12) and doing the mathematical simplifications, P_e^{RD} in (4.14) is written as

$$P_e^{RD} = \lambda \int_0^{\infty} G_{1,3}^{2,1}\left(\frac{\gamma}{\bar{\gamma}_D} \middle| {}^{1}_{0,0,1}\right) G_{2,3}^{2,1}\left(b\gamma \middle| {}^{1,1}_{0,0.5,1}\right) \mathrm{d}\gamma \tag{4.20}$$

where $\lambda = a/(2\bar{\gamma}_D\sqrt{\pi})$. Furhermore, by subsituting [45, eq.21], the P_e^{RD} is obtained as

$$P_e^{RD} = \frac{a}{2\sqrt{\pi}} G_{5,4}^{3,3}\left(b\bar{\gamma}_D \middle| {}^{1,0,0,-1,1}_{0,0.5,-1,1}\right). \tag{4.21}$$

Finally, the overall SEP for the considered system is obtained by substituting (4.19) and (4.21) in (4.14) using DF relaying protocol.

4.2.2 AF relaying protocol

In AF relaying protocol, since R applies the MRC technique, the CDF of the received SNR of the combined signal at R is given as [38]

$$F_{\gamma_R}(\gamma) = \frac{1}{\Gamma(k_L)\Gamma(m_L)} G_{1,3}^{2,1}\left(\frac{k_L m_L}{\bar{\gamma}_R}\gamma \middle| {}^{1}_{k_L, m_L, 0}\right). \tag{4.22}$$

The overall SEP performance of the considered system is calculated by substituting (4.11) in (4.13). Here, CDF of $F_{\gamma e2e}(\gamma)$ is calculated through by substituting (4.2) and (4.22) in (4.11). Meanwhile, under the assumption of $X \triangleq 2\sqrt{\frac{\gamma}{\bar{\gamma}_D}}\mathrm{K}_1\left(2\sqrt{\frac{\gamma}{\bar{\gamma}_D}}\right)$ and $Y \triangleq F_{\gamma_R}(\gamma)$, the CDF of the e2e received SNR expression in (4.11) becomes $F_{\gamma_{e2e}}(\gamma) =$

$Y+1-X-Y(1-X)=1-X+XY$. At this point, the overall SEP performance P_e of the system after applying $F_{\gamma_{e2e}}(\gamma)$ in (4.13), can be re-written as

$$P_e = \frac{a\sqrt{b}}{2\sqrt{\pi}}(I_1+I_2) \tag{4.23}$$

where $I_1=\int_0^\infty \frac{e^{-b\gamma}}{\sqrt{\gamma}}(1-X)d\gamma$ and $I_2=\int_0^\infty \frac{e^{-b\gamma}}{\sqrt{\gamma}}XYd\gamma$. By using [36, Eq.(6.614.4)] and [36, Eq.(3.361.2)], I_1 in (4.23) is calculated as

$$I_1=\sqrt{\frac{\pi}{b}}-\frac{\pi}{2\sqrt{b}}e^{\frac{1}{2b\bar{\gamma}_D}}\mathrm{W}_{-\frac{1}{2},\frac{1}{2}}\left(\frac{1}{b\bar{\gamma}_D}\right) \tag{4.24}$$

where $\mathrm{W}_{v,u}(\cdot)$ is Whittaker function [36]. Moreover, I_2 in (4.23) is obtained as

$$I_2=\zeta\int_0^\infty e^{-b\gamma}K_1\left(2\sqrt{\frac{\gamma}{\bar{\gamma}_D}}\right)G_{1,3}^{2,1}\left(\frac{k_Lm_L}{\bar{\gamma}_R}\gamma\Big|_{k_L,m_L,0}^{1}\right)\mathrm{d}\gamma \tag{4.25}$$

where $\zeta=\frac{2(\bar{\gamma}_D)^{-\frac{1}{2}}}{\Gamma(k_L)\Gamma(m_L)}$. Please note that, closed-form expression of I_2 is not available since the integral is not mathematically tractible. Thus, the results are evaluated numerically. Finally, the overall SEP performance of the AF relaying system is obtained by substituting (4.24) and (4.25) into (4.23).

Moreover, the average BEP performance of the considered system can be obtained by substituting the SEP as $P_e^{BEP}\approx P_e/log_2(M)$ where M represents the modulation parameter.

4.3 Numerical Results and Simulations

In this section, analytical derivations and simulation results are presented. The average power of fading channels are assumed as $E[|h_{SR_i}|^2]=E[|h_{RD}|^2]=1$ for $i\in\{1,2,\ldots,L\}$. Furthermore, modulation type is considered as 4-PSK where the parameters are determined as $a=2$ and $b=\sin^2(\frac{\pi}{4})$ in (4.12) and (4.13). Moreover, the average received SNR at each branch of the R is assigned equally, $\bar{\gamma}_1=\bar{\gamma}_2=\cdots=\bar{\gamma}_L$. As it is illustrated in Fig. 4.2 and 4.3, lines denotes the theoretical results while markers represents the simulation results.

The system performance is shown in terms of BEP analysis for DF relaying protocol scenario in Fig. 4.2. Since we investigate V2V communications, the channels are assumed as double Rayleigh fading for a multi-antenna relay-assisted system. As shown in Figure 4.2, BEP performance is increased for the system considered for

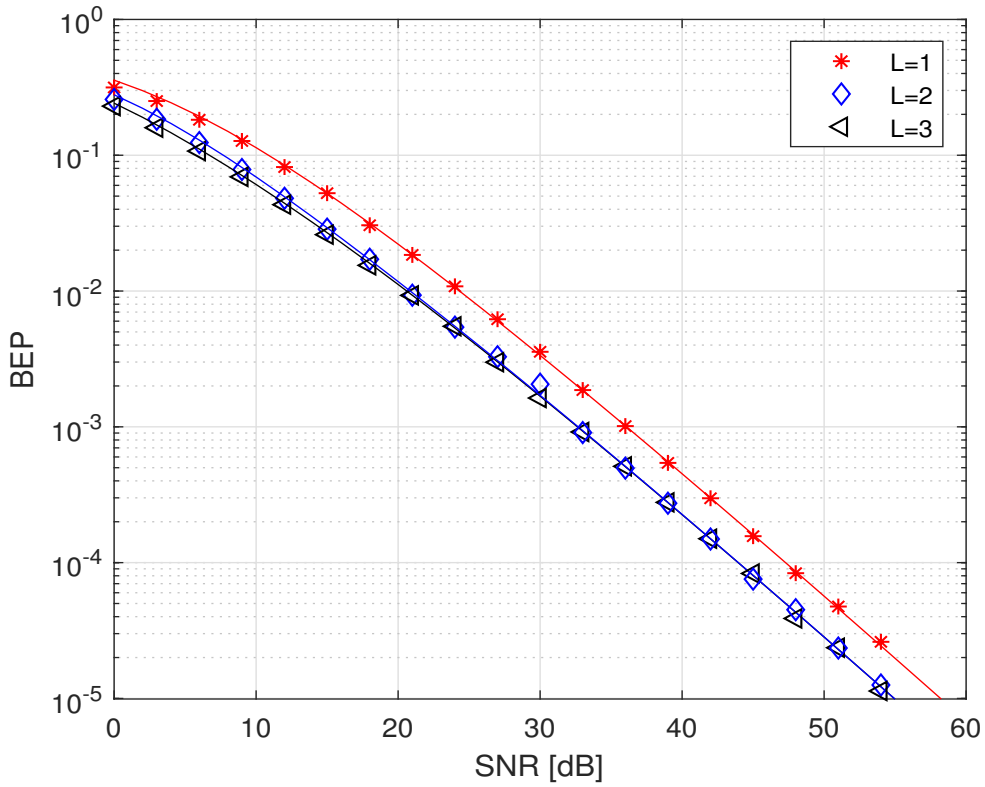

Figure 4.2 : The BEP performance for DF transmission protocol with the increasing number of antennas at R.

increasing R antenna number. The performance is substantially increased for $L = 2$ compared to the single antenna relay-assisted system $L = 1$.

The performance of AF relaying protocol versus SNR is considered in Fig. 4.3. As shown in the figure, system performance increases when the number of R antennas increases due to the diversity gain provided by the MRC technique.

Furthermore, the simulation results and theoretical analysis are verified with each other for both DF and AF relaying protocols. Meanwhile, the BEP performance at medium and high SNR values for both DF and AF protocols are considerably equivalent, and these results are consistent with the previous studies in the literature [46].

In this chapter, a cooperative V2V system is studied where the overall system performance are provided for both DF and AF relaying protocols in a V2V environment. Also, the results are provided for different system parameters. In the next section, performance of a cooperative vehicular networks considering physical layer security will be discussed.

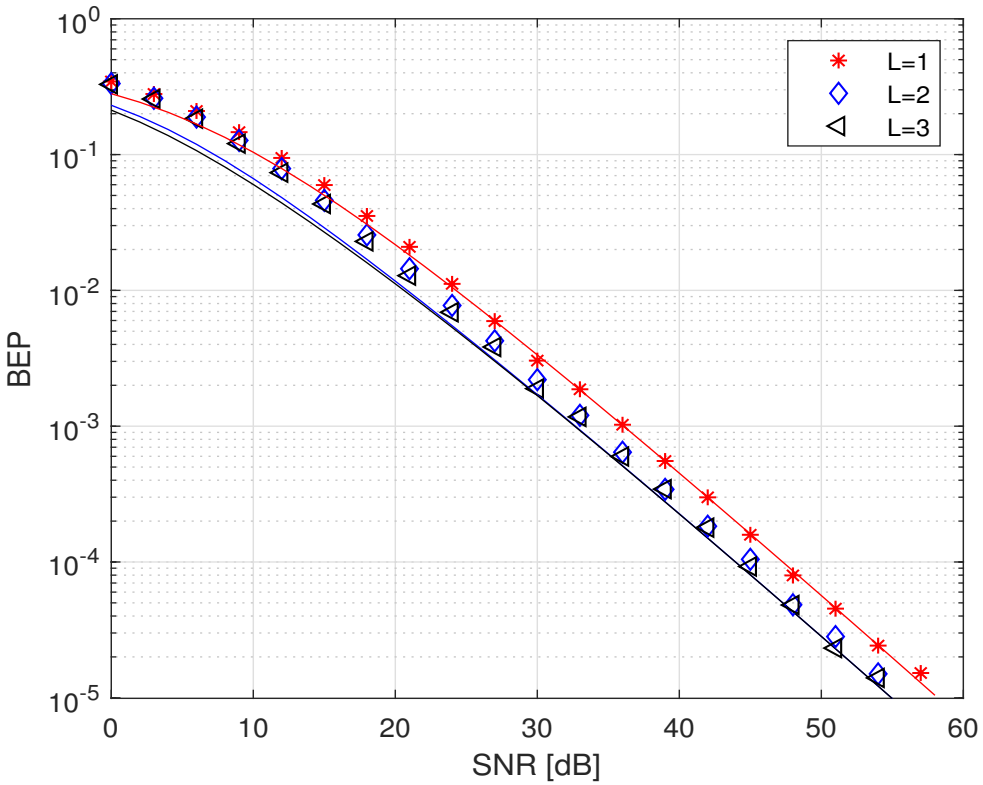

Figure 4.3 : The BEP performance for AF transmission protocol with the increasing number of antennas at R.

5. COOPERATIVE PHYSICAL LAYER SECURITY

Due to the nature of wireless communication, the signal is broadcasted to the entire environment. Thus, this information can be received by the illegitimate users in the communication range. Besides, more and more devices are expected to connect with each other in the next generation of wireless communications. Meanwhile, these connected devices can be over-headed by a non-legitimate users, which disregards privacy of the user and confidential information. Additionally, the numerous illegal cyberattacks are increasing everyday [47]. Thus, security is one of the important factors besides the reliability and low latency of next-generation communications. Among the open systems interconnection (OSI) model, security at the physical layer is the primary concern since it is located in the first layer of the OSI model architecture. Unlike other methods to improve security in the upper layers of the OSI model, solutions for eavesdropping and jamming attacks have been considered as a major issues in physical layer security.

5.1 Physical Layer Security Attack Types and Precautions

In the eavesdropping attack, the illegitimate users try to capture confidential information of legitimate user. Moreover, as long as the eavesdropper is located in coverage area of the source, it can acquire private information. Meanwhile, in the jamming attacks, a jammer interrupts the broadcasted signal to the legitimate users, which causes a low signal quality. In other words, this node deliberately generates an interference signal which interrupts the signal at the destination node. Furthermore, Fig. 5.1 shows several physical layer security (PLS) techniques studied in the literature to prevent illegal users from accessing the network [48].

Beamforming is a multi-antenna technique that allows a source node to transmit its information to a target node in a specific direction, causing illegitimate users to experience destructive effect of the transmitted signal. On the other hand, an artificial noise is generated by a transmitter and is added to null-subspace of the channel between

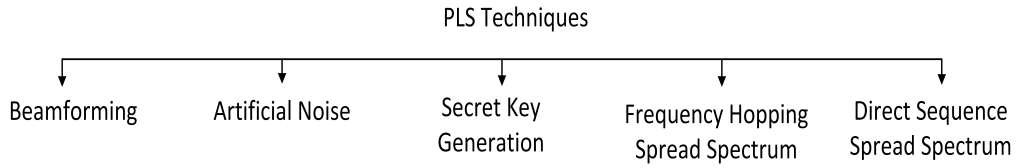

Figure 5.1 : PLS techniques.

transmitter and receiver nodes. This artificial noise adversely affects the performance of the illegitimate user, and it degrades the signal reception quality. Furthermore, both transmitter and receiver nodes can generate a secret key relying on the channel state information (CSI) of the channel between them using the randomness of the physical layer characteristic. Thus, this technique ensures that the transmitted data remains confidential between source and destination since illegal users cannot obtain the CSI of the legitimate link of users [49]. Frequency-hopping spread spectrum (FHSS) is another technique for preventing physical layer attacks. In FHSS, the carrier frequency is immediately replaced by a predefined frequency hopping pattern across a broad spectrum. This method prevents the jammer from affecting the signal quality. Besides, in direct sequence spread spectrum (DSSS), the transmitter intentionally spreads the generated signal over a broader bandwidth that avoids jamming attacks. This technique provides secure communication and improves system quality.

5.2 Performance Analysis of Cooperative Physical Layer Security for V2V

In this section, PLS analysis of a cooperative wireless communication system is proposed. In this system, source and destination nodes communicate via a relay, and a direct link between source and relay does not exist. Meanwhile, the relay node applies the decode-and-forward (DF) relaying protocol. Source, relay and destination nodes are equipped with a single antenna. Since all of the nodes are mobile, channel fading coefficients are assumed as double Rayleigh. Furthermore, an eavesdropper illegitimately accesses transmitted information of the source and relay with multiple antennas by applying the maximum ratio combining (MRC) technique. This causes eavesdropper to have more intention to obtain information from legitimate user. Theoretical expressions of secrecy outage probability (SOP) and the probability of positive secrecy capacity (PPSC) analysis of the considered system are obtained in closed-form and theoretical results are verified by Monte-Carlo simulation results.

5.2.1 System model

In the V2V communication system shown in the Fig. 5.2, there is no direct connection between the source (S) and destination (D) nodes and their communication is provided in two-time slots via the relay (R) applying the DF relaying protocol. Moreover, the illegitimate user, eavesdropper (E), tries to access the transmitted information from S to D when E is close to S. In other words, E can illegitimately listen to signals from both S and R. E has the advantage of having multiple antennas that can apply the MRC scheme to acquire the transmitted information illegally. To the best of the author's knowledge, this model has not been studied in the literature yet. Furthermore, the channel models between all the links are assumed as double Rayleigh fading since all the nodes are mobile in the wireless environment. Accordingly, the probability density function (PDF) and cumulative distribution function (CDF) of the instantaneous signal-to-noise ratio (SNR) of γ observed in the channels, respectively, are given as

$$p_{\gamma}(\gamma) = \frac{2}{\bar{\gamma}} \mathrm{K}_0 \left(2\sqrt{\frac{\gamma}{\bar{\gamma}}} \right), \tag{5.1}$$

$$F_{\gamma}(\gamma) = 1 - 2\sqrt{\frac{\gamma}{\bar{\gamma}}} K_1 \left(2\sqrt{\frac{\gamma}{\bar{\gamma}}} \right) \tag{5.2}$$

where $K_{\nu}(.)$ is the $\nu-$th order modified Bessel function [36] and $\bar{\gamma}$ represents average instantaneous received SNR. Within the scope of PLS of the proposed system, the secrecy capacity is expressed as [9]

$$C_{sec} = |C_D - C_E|^{+} \tag{5.3}$$

where $C_x = \frac{1}{2}\log(1+\gamma_x)$ is the capacity of the user x for $x \in \{D, E\}$. Here, γ_x is the end-to-end received SNR at the related receive nodes. Assuming DF relaying protocol,

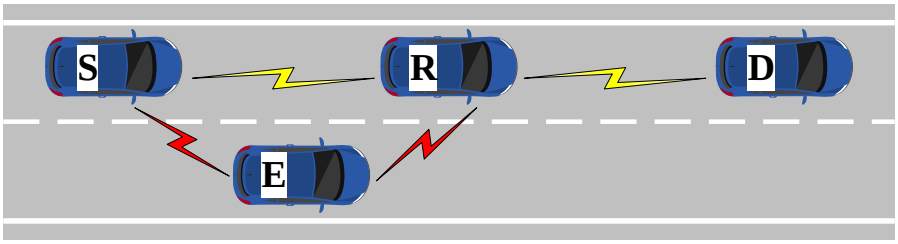

Figure 5.2 : Cooperative V2V communication system employing DF relaying with PLS technique.

capacity of the system is given as

$$C_D = \min(C_{SR}, C_{RD}) \tag{5.4}$$

where C_{SR} and C_{RD} are the data transmission capacities of the links between S-R and R-D, respectively. On the other hand, E will listen to both S and R while using the MRC technique with multiple antennas to achieve diversity gain, so the received SNR at E is expressed as

$$\gamma_{yE} = \sum_{l=1}^{L} \gamma_{yE_l} \tag{5.5}$$

where $y = S$ and $y = R$ are for links S→E and R→E, respectively. Moreover, L represents the number of antennas of E. When the source is $y = S$, the instantaneous SNR obtained by $l-$th antenna of E is represented as γ_{SE_l}.

Please note that, the PDF of the SNR over double Rayleigh fading channels can be expressed a special case of Gamma-Gamma distribution which is given as [38]

$$p_\gamma(\gamma) = \frac{2(km)^{\frac{k+m}{2}} \gamma^{\frac{k+m}{2}-1}}{\Gamma(k)\Gamma(m)\bar{\gamma}^{\frac{k+m}{2}}} K_{k-m}\left(2\sqrt{\gamma/\bar{\gamma}}\right) \tag{5.6}$$

for $k = m = 1$. Since the sum of identically distributed Gamma-Gamma random variables is also shown to be a Gamma-Gamma distributed random variable [38], the PDF of γ_{yE} in (5.5) is expressed as

$$p_{\gamma_{yE}}(\gamma) = \frac{2(k_L m_L)^{\alpha} \gamma^{\alpha-1}}{\Gamma(k_L)\Gamma(m_L)\bar{\gamma}_{yE}^{\alpha}} K_{k_L-m_L}\left(2\sqrt{\frac{k_L m_L}{\bar{\gamma}_{yE}}\gamma}\right) \tag{5.7}$$

where $\alpha = \frac{k_L+m_L}{2}$, $k_L = Lk + (L-1)\frac{-0.127-0.95k-0.0058m}{1+0.00124k+0.98m}$, $m_L = Lm$ and $\bar{\gamma}_{yE} = L\gamma_{yE_l}$ for $l = 1, ..., L$. For double Rayleigh case, $k = m = 1$ [38].

5.2.2 Secrecy outage probability analysis

In order to guarantee complete privacy when E is a illegitimate user in the system, the instantaneous secrecy capacity C_{sec} must be greater than the fixed R_s data rate. Otherwise, secrecy will not be ensured in terms of information theory in the system. SOP, which is defined as a measure of this situation, is given as

$$SOP = \Pr\{C_D < R_s\}. \tag{5.8}$$

Additionally, applying the equation (5.4) in (5.8), SOP is simplified as

$$\begin{aligned} SOP &= \Pr\{\min(C_{SR}, C_{RD}) < R_s\} \\ &= 1 - \Pr\{\min(C_{SR}, C_{RD}) \geq R_s\} \\ &= 1 - \Pr\{C_{SR} \geq R_s\} \Pr\{C_{RD} \geq R_s\}. \end{aligned} \tag{5.9}$$

Calculation of $\Pr\{C_{SR} \geq R_s\}$ and $\Pr\{C_{RD} \geq R_s\}$ are given in (5.2.2.1) and (5.2.2.2), respectively.

5.2.2.1 Calculation of $\Pr\{C_{SR} \geq R_s\}$

In this part, we calculate $\Pr\{C_{SR} \geq R_s\}$ in (5.9). In the first time slot, while S broadcasts its signal, the channel secrecy capacity between S→R is given as

$$C_{SR} = \frac{1}{2}\log_2(1+\gamma_{SR}) - \frac{1}{2}\log_2(1+\gamma_{SE}) \tag{5.10}$$

where γ_{SR} ve γ_{SE} are the instantaneous received SNR at nodes R and E, respectively. Please note that the factor "$1/2$" corresponds to two transmission time slot. Substituting (5.10) in the first term of the right side of the equation in (5.9), we have

$$\begin{aligned} \Pr\{C_{SR} \geq R_s\} &= \Pr\{\log_2\left(\frac{1+\gamma_{SR}}{1+\gamma_{SE}}\right) \geq 2R_s\} \\ &= \Pr\{\gamma_{SR} \geq a\gamma_{SE} + a - 1\} \\ &= 1 - \Pr\{\gamma_{SR} < a\gamma_{SE} + a - 1\} \\ &\approx 1 - \Pr\{\gamma_{SR} < a\gamma_{SE}\} \\ &= 1 - \int_0^\infty F_{\gamma_{SR}}(a\gamma)\, p_{\gamma_{SE}}(\gamma)\, d\gamma \end{aligned} \tag{5.11}$$

where $a = 2^{2R_s}$, $F_{\gamma_{SR}}(a\gamma)$ is the CDF of link S→R and $p_{\gamma_{SE}}(\gamma)$ is the PDF of link S→E. Please note that, we assume a tight upper bound $a\gamma_{SE} \gg a - 1$. Substituting (5.2) in (5.11), we have

$$\begin{aligned} Pr\{C_{SR} \geq R_s\} &= 1 - \int_0^\infty (1-X)\, p_{\gamma_{SE}}(\gamma)\, d\gamma \\ &= 1 - \int_0^\infty p_{\gamma_{SE}}(\gamma)\, d\gamma + \int_0^\infty X p_{\gamma_{SE}}(\gamma)\, d\gamma \\ &= \int_0^\infty X p_{\gamma_{SE}}(\gamma)\, d\gamma \end{aligned} \tag{5.12}$$

where $X = 2\sqrt{\frac{a\gamma}{\bar{\gamma}_{SR}}} K_1\left(2\sqrt{\frac{a\gamma}{\bar{\gamma}_{SR}}}\right)$. By substituting (5.7) into (5.12), we obtain

$$\Pr\{C_{SR} \geq R_s\} = 2\varepsilon\sqrt{\frac{a}{\bar{\gamma}_{SR}}} \int_0^\infty \gamma^{\alpha-0.5} K_1\left(2\sqrt{\frac{a\gamma}{\bar{\gamma}_{SR}}}\right) K_{k_L-m_L}\left(2\sqrt{\frac{k_L m_L \gamma}{\bar{\gamma}_{SE}}}\right) d\gamma \tag{5.13}$$

where $\varepsilon = \frac{2(k_L m_L)^{\alpha}}{\Gamma(k_L)\Gamma(m_L)\bar{\gamma}_{SE}^{\alpha}}$. Using [45, 14] and [36, 9.31-1], (5.13) is obtained as

$$\Pr\{C_{SR} \geq R_s\} = \frac{\varepsilon}{2}\sqrt{\frac{a}{\bar{\gamma}_{SR}}}\int_0^{\infty} \gamma^{\alpha-0.5} G_{1,3}^{2,1}\left(\frac{a\gamma}{\bar{\gamma}_{SR}}\middle|_{0.5,-0.5,1}^{1}\right) \times G_{1,3}^{2,1}\left(\frac{k_L m_L \gamma}{\bar{\gamma}_{SE}}\middle|_{\beta,-\beta,1}^{1}\right) d\gamma \tag{5.14}$$

where $G_{p,q}^{m,n}(.|.)$ is a Meijer's-G function [36, 9.31.1] and $\beta = \frac{k_L - m_L}{2}$. Finally, using [45, 21] and re-writing (5.14), close-form expression is given as

$$\Pr\{C_{SR} \geq R_s\} = \frac{\varepsilon}{2}\left(\frac{\bar{\gamma}_{SR}}{a}\right)^{\alpha} G_{4,4}^{3,3}\left(\frac{k_L m_L \bar{\gamma}_{SR}}{a\bar{\gamma}_{SE}}\middle|_{\beta,-\beta,-\alpha-0.5,1}^{1,-\alpha,1-\alpha,-\alpha-0.5}\right). \tag{5.15}$$

5.2.2.2 Calculation of $\Pr\{C_{RD} \geq R_s\}$

In this part, we calculate $\Pr\{C_{RD} \geq R_s\}$ in (5.9). The channel secrecy capacity in link R→D is

$$C_{RD} = \frac{1}{2}\log_2(1+\gamma_{RD}) - \frac{1}{2}\log_2(1+\gamma_{RE}) \tag{5.16}$$

where γ_{RD} and γ_{RE} are the instantaneous received SNR respectively in nodes D and E while R applies DF relaying protocol in the second phase of the transmission of the system. Here, following the same procedure as done in (5.2.2.1), we have

$$\Pr\{C_{RD} \geq R_s\} = \frac{\varepsilon'}{2}\left(\frac{\bar{\gamma}_{RD}}{a}\right)^{\alpha} G_{4,4}^{3,3}\left(\frac{k_L m_L \bar{\gamma}_{RD}}{a\bar{\gamma}_{RE}}\middle|_{\beta,-\beta,-\alpha-0.5,1}^{1,-\alpha,1-\alpha,-\alpha-0.5}\right) \tag{5.17}$$

where $\varepsilon' = \frac{2(k_L m_L)^{\alpha}}{\Gamma(k_L)\Gamma(m_L)\bar{\gamma}_{RE}^{\alpha}}$. Finally, the SOP expression of the system is obtained in closed-form by substituting (5.15) and (5.17) in (5.9).

5.2.3 PPSC performance evaluation

In wireless communication, while considering the positive PLS performance of the system, there is always an instantaneous secrecy capacity, which is called as the PPSC. PPSC is expressed as

$$PPSC = \Pr\{C_{sec} > 0\}. \tag{5.18}$$

Accordingly, considering DF relaying protocol and using (5.4), PPSC is expressed as

$$PPSC = \Pr\{\min(C_{SR}, C_{RD}) > 0\}. \tag{5.19}$$

Meanwhile, PPSC can be calculated in terms of derived SOP in (5.8) as

$$PPSC = 1 - SOP(R_s = 0) \tag{5.20}$$

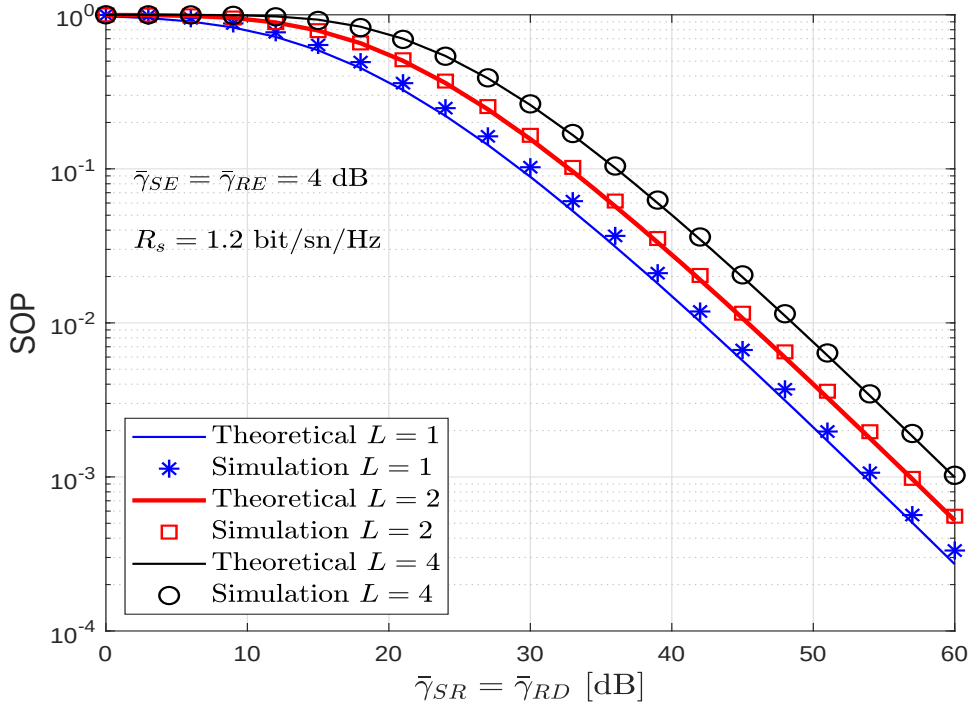

Figure 5.3 : SOP comparison of double Rayleigh fading channels for the number of eavesdropper antennas $L = 1, 2$ and 4.

5.2.4 Simulations and numerical results

In this part, the theoretical analyses are verified with Monte-Carlo simulation methods. It is assumed that S and R nodes are broadcasting signals with unit transmit power. Moreover, the average channel gains between links S→R and R→D are also assumed with unit power ($\Omega_{SR} = \Omega_{RD} = 1$). Furthermore, channel distributions between S-E and R-E are accepted as i.i.d in analytical calculations and simulations.

In Fig. 5.3, the SOP performance of the system is given when all the channel fading are assumed as double Rayleigh distribution according to the number of different antennas in illegitimate node E. Simulations are performed for $L = 1, 2$ and 4. Data transmission rate is fixed at $R_s = 1.2$ bit/sec/Hz and the average SNR observed at E is assumed as $\bar{\gamma}_{SE} = \bar{\gamma}_{RE} = 4$ dB. It is shown in the figure that SOP performance is decreasing as the number of the antenna at E increases.

Fig. 5.4 denotes the SOP versus $\bar{\gamma}_{SR} = \bar{\gamma}_{RD}$. The results are provided for different values of $\bar{\gamma}_{SE}$ and $\bar{\gamma}_{SE}$. Here, the data transmission rate is assumed to be $R_s = 1.2$ bits/sec/Hz and the number of receiving antennas of E is $L = 2$. In these conditions, it is observed that PLS performance improved in a V2V communication system with DF relaying in

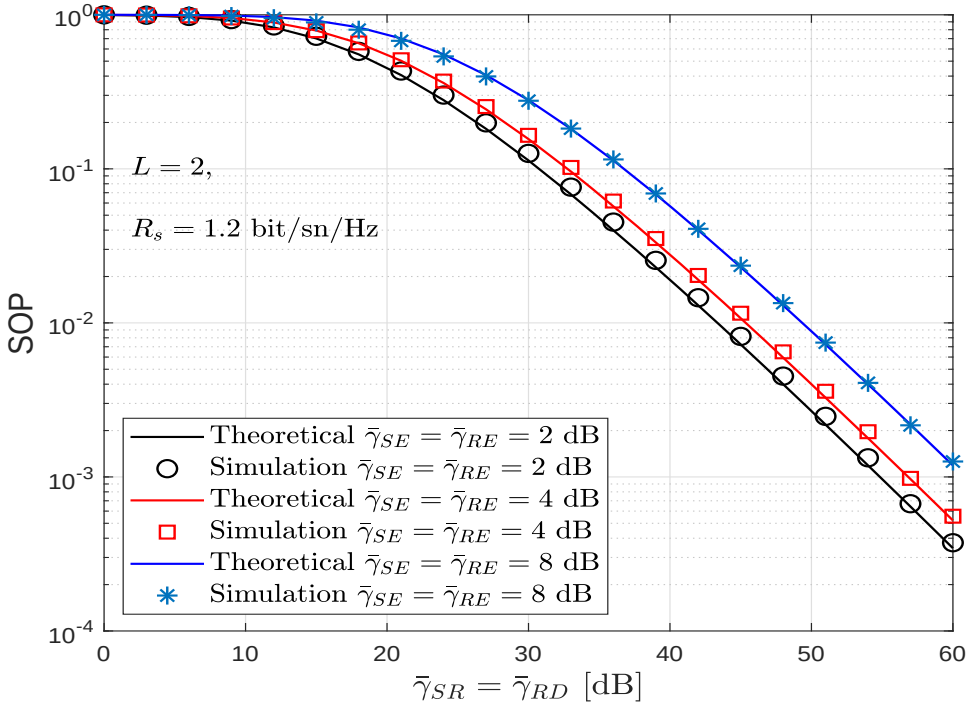

Figure 5.4 : SOP performance comparison for double Rayleigh fading channels for $\bar{\gamma}_{SE} = \bar{\gamma}_{RE} = 2, 4$ ve 8 dB.

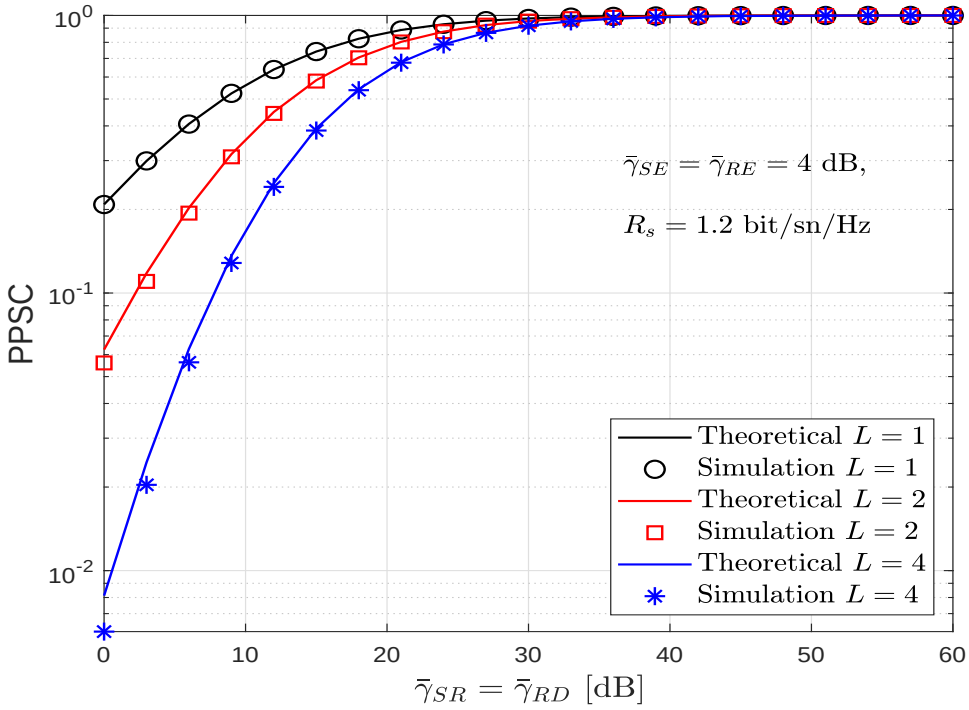

Figure 5.5 : PPSC performance comparison for double Rayleigh fading channels when antenna number of E is $L = 1, 2$ ve 4.

double Rayleigh fading channels due to the decrease in the average SNR obtained in E and the SOP in the legitimate user is decreased.

Fig. 5.5 shows the effect of E antenna number ($L = 1, 2$ and 4) on PPSC performance. Here, it is assumed that $\bar{\gamma}_{SE} = \bar{\gamma}_{RE} = 4$ dB. As shown in Fig 5.5 , as the number of antennas increases, PPSC decreases in accordingly with SOP performance.

As is indicated in all the figures, the theoretical results are consistent with the Monte-Carlo simulation results and matched perfectly.

In this chapter, we study the SOP and PPSC of the cooperative DF relaying protocol. Here, we assume a mobile eavesdropper equipped with multiple antenna where intercept the confidential information of the legitimate user. In the next chapter, due to the spectrum scarcity of the wireless communications, non-orthogonal multiple access technique is studied in cooperative vehicular networks.

6. COOPERATIVE NON-ORTHOGONAL MULTIPLE ACCESS (NOMA)

Mobile communication data traffic is increasing in recent years. Usually, users access the available spectrum simultaneously by dividing them via the orthogonal multiple access (OMA) technique. However, due to the demand for higher data rates in next-generation wireless communications, spectrum scarcity will be encountered. Meanwhile, non-orthogonal multiple access (NOMA) is recognized as a promising multiple access technique for next-generation wireless networks that improves spectral efficiency and ensures user fairness. Besides, NOMA simultaneously uses the same frequency band or time interval to enable users to achieve higher bandwidth efficiency.

The NOMA technique can be categorized as downlink and uplink corresponding to transmission from a base station (BS) to users or vice versa. Furthermore, this technique can also be categorized as a power domain or code domain that allocates the power for users or splits the signal as a code. In this thesis, we focus on the downlink power domain NOMA.

6.1 Principles of Power Domain NOMA

In the downlink power domain NOMA, BS transmits its signal to users using superposition coding. In other words, all users operate in the same frequency and symbol of each user is transmitted with predefined power which is depending on the channel condition. Besides, users decode their signals using the successive interference cancellation (SIC) method, considering signals of other users as an interference.

6.1.1 Superposition coding

In this technique, BS broadcasts the information for each user with different power allocation. In two-user assisted NOMA system, for the weak user more power is allocated and for the strong user less power is allocated which provide user fairness. The transmitted signal from the BS is given as

$$x = \sqrt{P_1}\, s_1 + \sqrt{P_2}\, s_2. \tag{6.1}$$

where s_i is the transmitted signal and $P_i = \alpha_i P_t$ is the allocated power for individual users where $i \in \{1,2\}$. At this point, α_i is the power allocation coefficient where $\alpha_1 + \alpha_2 = 1$ and P_t is the total transmit power of the BS. Here, channels are ordered as $|h_1|^2 < |h_2|^2$. The received signal at each user is expressed as

$$y_i = \sqrt{P_t} h_i x + n_i \tag{6.2}$$

where n_i is the sampled complex white Gaussian noise with zero mean and N_0 variance.

6.1.2 SIC technique

In two-user NOMA based systems, the signal of the weak user will be more dominant over the signal of the strong user. So, the signal of U_1 perceived as interference, and no SIC is required. Thus, the weak user decodes its signal directly. At this point, the received signal-to-interference and noise ratio (SINR) at the weak user is given as

$$\gamma_1 = \frac{P_1 |h_1|^2}{P_2 |h_1|^2 + N_0}. \tag{6.3}$$

However, when the signal is transmitted from the strong channel, the user with high power is first decoded using SIC. The SINR expression is given as

$$\gamma_{1,2} = \frac{P_1 |h_2|^2}{P_2 |h_2|^2 + N_0}. \tag{6.4}$$

This decoded signal is omitted from the transmitted signal, and the interference is canceled. Consequently, the user decodes its signal without interference. The receiver signal-to-noise ratio (SNR) at the strong user is calculated as

$$\gamma_2 = \frac{P_2 |h_2|^2}{N_0}. \tag{6.5}$$

6.2 NOMA-based Cooperative V2V Communications

A cooperative power-domain downlink NOMA system is presented in Fig. 6.1. The system is consists of a BS, a relay (R), and two paired users. Additionally, users are also denoted as U_1 (strong user) and U_2 (weak user) for simplicity. Moreover, it is assumed that all nodes are equipped with a single antenna, and the system operates in half-duplex mode. Here it is assumed that no direct link is available from BS to both users, and R provides the transmission from BS to both users. In other words, R increases the coverage area of the BS. This condition is faced when the two mobile

users are near the cell edge, and the direct link is in the deep fade. As shown in Fig. 6.1, h_r, h_1, and h_2 represents the channel fading of the links BS→R, R→U_1 and R→U_2, respectively. Moreover, the links between mobile nodes R→U_1 and R→U_2 are exposed to double Rayleigh fading, which is the product of two Rayleigh fading [33]. Besides, we assume that the link BS→R is exposed to Rayleigh fading.

Furthermore, channel gains are denoted as $E\left[|h_i|^2\right] = \Omega_i$ for $i \in \{1,2\}$ and the channels $|h_1|^2$ and $|h_2|^2$ are ordered as $|h_1|^2 \geq |h_2|^2$. Additionally, s_1 and s_2 are the signals of U_1 and U_2, respectively. Moreover, n_x represents the complex additive Gaussion noise with zero mean and N_0 variance as $\mathscr{CN}(0, N_0)$ for $x \in \{r,1,2\}$.

The data transmission occurs in a two-time slot where R applies a fixed-gain amplify-and-forward (AF). In the first transmission slot, BS transmits the superimposed signal of both s_1 and s_2 to node R as

$$x = \sqrt{P_1}\, s_1 + \sqrt{P_2}\, s_2. \tag{6.6}$$

where $P_1 = \alpha_1 P_t$ and $P_2 = \alpha_2 P_t$ are the allocated power for U_1 and U_2 users signal. Here, P_t is the total transmit power of BS and α_i is the power allocation coefficient where $\alpha_1 + \alpha_2 = 1$. In NOMA, more power is assigned to weak user (U_2) than the strong user (U_1) where $\alpha_1 < \alpha_2$. The received signal at R is written as

$$y_r = h_r x + n_r = h_r(\sqrt{P_1}s_1 + \sqrt{P_2}s_2) + n_r. \tag{6.7}$$

Furthermore, in the second time slot, the R applies AF relaying protocol. The received signal at the $i-$th user is given as

$$y_i = G h_i y_r + n_i = G h_i h_r \underbrace{\left(\sqrt{P_1}s_1 + \sqrt{P_2}s_2\right)}_{\text{Broadcasted signal from BS}} + \underbrace{G h_i n_r + n_i}_{\text{Noise}} \tag{6.8}$$

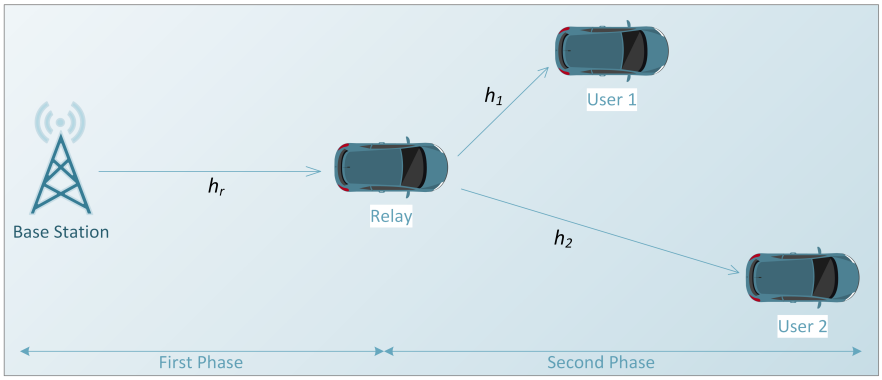

Figure 6.1 : NOMA-based two-user assisted cooperative V2V communication system model.

where $i \in \{1,2\}$ and $G = \sqrt{P_r/\left(P_t E\left[|h_r|^2\right] + N_0\right)}$ is the scaling normalization factor. Applying the perfect SIC process at node U_1, the received SINR of the U_2 corresponding to s_2 signal at node U_1 is calculated as

$$\gamma_{1,2} = \frac{G^2|h_1|^2|h_r|^2 P_2}{G^2|h_1|^2|h_r|^2 P_1 + G^2|h_1|^2 N_0 + N_0}. \tag{6.9}$$

After successfully decoding the s_2 signal at U_1, consequently, U_1 neglects the decoded signal from (6.8). So, the received SNR at U_1 is expressed as

$$\gamma_1 = \frac{G^2|h_1|^2|h_r|^2 P_1}{G^2|h_1|^2 N_0 + N_0}. \tag{6.10}$$

Finally, the received SINR at node U_2 is calculated from (6.8) and $i = 2$ as

$$\gamma_2 = \frac{G^2|h_2|^2|h_r|^2 P_2}{G^2|h_2|^2|h_r|^2 P_1 + G^2|h_2|^2 N_0 + N_0}. \tag{6.11}$$

6.2.1 Outage probability analysis

In this part, the outage probability of a cooperative NOMA-based AF relaying system is investigated, and theoretical expressions for both users and the overall system are derived.

6.2.1.1 Outage probability of U_1

The outage probability of U_1 occurs when the instantaneous received SNR at (6.9) and (6.10) are smaller than the pre-defined thresholds. In this case, the outage probability of the near user (U_1) is expressed as

$$P_{out}^1 = 1 - \Pr\{\gamma_{1,2} > \gamma_{th_2}, \gamma_1 > \gamma_{th_1}\} \tag{6.12}$$

where $\gamma_{th_1} = 2^{2R_1} - 1$ and $\gamma_{th_2} = 2^{2R_2} - 1$. Here, R_1 and R_2 are the corresponding target date rates at U_1 and U_2, respectively. Substituting (6.9) and (6.10) in (6.12), the outage probability is re-expressed as

$$P_{out}^1 = 1 - \Pr\left\{\frac{G^2|h_1|^2|h_r|^2 P_2}{G^2|h_1|^2|h_r|^2 P_1 + G^2|h_1|^2 N_0 + N_0} > \gamma_{th_2}, \frac{G^2|h_1|^2|h_r|^2 P_1}{G^2|h_1|^2 N_0 + N_0} > \gamma_{th_1}\right\}. \tag{6.13}$$

After some mathematical simplification, (6.13) is calculated as

$$P_{out}^1 = 1 - \Pr\left\{|h_1|^2 G^2\left(|h_r|^2\left(P_2 - P_1\gamma_{th_2}\right) - \rho_2\right) > \rho_2, |h_1|^2 G^2\left(|h_r|^2 P_1 - \rho_1\right) > \rho_1\right\}. \tag{6.14}$$

where $\rho_1 = N_0\gamma_{th_1}$ and $\rho_2 = N_0\gamma_{th_2}$. Since all the channel fading parameters are independent and identically distributed (i.i.d), the outage probability P_{out}^1 in (6.14) is re-written as

$$P_{out}^1 = 1 - \Pr\left\{|h_r|^2 > \tau, |h_1|^2 > \left(\frac{\tau/G^2}{|h_r|^2 - \tau}\right)\right\} \Pr\left\{|h_r|^2 > \upsilon, |h_1|^2 > \left(\frac{\upsilon/G^2}{|h_r|^2 - \upsilon}\right)\right\} \tag{6.15}$$

where $\tau \stackrel{\triangle}{=} \rho_2/(P_2 - P_1\gamma_{th_2})$ and $\upsilon \stackrel{\triangle}{=} \rho_1/P_1$. Please note that $\gamma_{th_2} < P_2/P_1$. Unless otherwise stated P_{out}^1 is equal to one. Additionally, for simplicity of calculation, (6.15) is re-expressed as

$$P_{out}^1 = 1 - \Pr\left\{|h_r|^2 > \max(\tau, \upsilon) \stackrel{\triangle}{=} \phi, |h_1|^2 > \frac{\phi/G^2}{|h_r|^2 - \phi}\right\} \tag{6.16}$$

$$= 1 - \int_{\phi}^{\infty} p_{|h_r|^2}(y) \int_{\frac{\phi/G^2}{y-\phi}}^{\infty} p_{|h_1|^2}(x)\, \mathrm{d}x\, \mathrm{d}y$$

$$= \int_{0}^{\phi} p_{|h_r|^2}(y)\, \mathrm{d}y + \int_{\phi}^{\infty} p_{|h_r|^2}(y)\, F_{|h_1|^2}\left(\frac{\phi/G^2}{y-\phi}\right) \mathrm{d}y. \tag{6.17}$$

where $p_{|h_r|^2}(\gamma)$ is the exponentially distributed random variable and is given as [34]

$$p_{|h_r|^2}(\gamma) = \frac{1}{\bar{\gamma}_r} \exp\left(\frac{\gamma}{\bar{\gamma}_r}\right). \tag{6.18}$$

where $\bar{\gamma}_r = \Omega_r$. Moreover, the link between R→U$_1$ is exposed to double Rayleigh fading. Thus, the corresponding cumulative distribution function (CDF) of the unordered channel fading is given as [7]

$$F_{|\tilde{h}_i|^2}(\gamma) = 1 - 2\sqrt{\frac{\gamma}{\bar{\gamma}_i}} \mathrm{K}_1\left(2\sqrt{\frac{\gamma}{\bar{\gamma}_i}}\right) \tag{6.19}$$

where $\mathrm{K}_v(.)$ is the $v-$th order modified Bessel function of the second kind [36], $\bar{\gamma}_i = \Omega_i$ is the corresponding average channel gain for $i \in \{1,2\}$. Considering order statistic from [50], the ordered distribution of CDF for U$_1$ is written as

$$F_{|h_i|^2}(\gamma) = \sum_{k=0}^{M-l} \frac{(-1)^k M!}{(l+k)(M-l-k)!(l-1)!k!} \left[F_{|\tilde{h}_i|^2}(\gamma)\right]^{l+k} \tag{6.20}$$

where for our case $M = 2$, $l = 2$ and $i = 1$. Substituting (6.19) in (6.20), the ordered CDF expression for close user is expressed as

$$F_{|h_1|^2}(\gamma) = \left[F_{|\tilde{h}_1|^2}(\gamma)\right]^2$$

$$= 1 - \omega_1(\gamma, \bar{\gamma}_1) + \omega_2(\gamma, \bar{\gamma}_1) \tag{6.21}$$

where

$$\omega_1(\gamma,\bar{\gamma}_1) = 4\sqrt{\frac{\gamma}{\bar{\gamma}_1}}\mathrm{K}_1\left(2\sqrt{\frac{\gamma}{\bar{\gamma}_1}}\right), \tag{6.22a}$$

$$\omega_2(\gamma,\bar{\gamma}_1) = 4\,\frac{\gamma}{\bar{\gamma}_1}\left[\mathrm{K}_1\left(2\sqrt{\frac{\gamma}{\bar{\gamma}_1}}\right)\right]^2 \tag{6.22b}$$

and $\bar{\gamma}_1 = \Omega_1$. Here, for simplicity, we assume that $\omega_1(\gamma,\bar{\gamma}_1)$ and $\omega_2(\gamma,\bar{\gamma}_1)$ are the functions of γ and $\bar{\gamma}_1$. Moreover, substituting (6.21) in (6.17), P_{out}^1 in (6.17) is written as

$$P_{out}^1 = 1 - \underbrace{\int_{\phi}^{\infty} p_{|h_r|^2}(\gamma)\,\omega_1\left(\frac{\phi/G^2}{\gamma-\phi},\bar{\gamma}_1\right)\mathrm{d}\gamma}_{I_1} + \underbrace{\int_{\phi}^{\infty} p_{|h_r|^2}(\gamma)\,\omega_2\left(\frac{\phi/G^2}{\gamma-\phi},\bar{\gamma}_1\right)\mathrm{d}\gamma}_{I_2}. \tag{6.23}$$

Now, substituting (6.22a) and (6.22b) in (6.23), I_1 in (6.23) is written as

$$I_1 = \int_{\phi}^{\infty} 4\sqrt{\frac{1}{\bar{\gamma}_1}\frac{\phi/G^2}{\gamma-\phi}}\mathrm{K}_1\left(2\sqrt{\frac{1}{\bar{\gamma}_1}\frac{\phi/G^2}{\gamma-\phi}}\right)\frac{1}{\bar{\gamma}_r}\exp\left(-\frac{\gamma}{\bar{\gamma}_r}\right)\mathrm{d}\gamma. \tag{6.24}$$

Furthermore, we assume that $\gamma-\phi = t$. Thus, (6.24) is re-expressed as

$$I_1 = 4\,\kappa_1\sqrt{\frac{\phi/G^2}{\bar{\gamma}_1}}\int_0^{\infty} t^{-\frac{1}{2}}\exp\left(-\frac{t}{\bar{\gamma}_r}\right)\mathrm{K}_1\left(2\sqrt{\frac{1}{\bar{\gamma}_1}\frac{\phi/G^2}{t}}\right)\mathrm{d}t \tag{6.25}$$

where $\kappa_1 = \frac{1}{\bar{\gamma}_r}\exp\left(-\frac{\phi}{\bar{\gamma}_r}\right)$. By using [45, 14], [36, 9.31-1], [36, 9.31-2] and [36, 9.31-5], (6.25) can be expressed as

$$I_1 = 2\,\kappa_1\int_0^{\infty} t^{-\frac{1}{2}}\exp\left(-\frac{t}{\bar{\gamma}_r}\right)G_{3,1}^{1,2}\left(t\frac{\bar{\gamma}_1}{\phi/G^2}\middle|\begin{matrix}\frac{1}{2},\frac{3}{2},0\\0\end{matrix}\right)\mathrm{d}t. \tag{6.26}$$

where $G_{p,q}^{m,n}(.|:)$ denotes Meijer's G-function [36]. Applying [36, 7.813-1] in (6.26), the closed-form solution for I_1 is calculated as

$$I_1 = 2\exp\left(-\frac{\phi}{\bar{\gamma}_r}\right)\,G_{4,1}^{1,3}\left(\frac{\bar{\gamma}_1\bar{\gamma}_r}{\phi/G^2}\middle|\begin{matrix}0,0,1,-\frac{1}{2}\\-\frac{1}{2}\end{matrix}\right). \tag{6.27}$$

By substituting (6.22b) in the third term on the right hand side of (6.23), I_2 is expressed as

$$I_2 = \int_{\phi}^{\infty}\frac{4}{\bar{\gamma}_1}\frac{\phi/G^2}{\gamma-\phi}\left[\mathrm{K}_1\left(2\sqrt{\frac{1}{\bar{\gamma}_1}\frac{\phi/G^2}{\gamma-\phi}}\right)\right]^2\frac{1}{\bar{\gamma}_r}\exp\left(-\frac{\gamma}{\bar{\gamma}_r}\right)\mathrm{d}\gamma. \tag{6.28}$$

For simplifying calculation process, we assume that $\gamma-\phi = t$. After some mathematical simplification, (6.28) is re-written as

$$I_2 = \kappa_1\int_0^{\infty}\frac{4\phi/G^2}{\bar{\gamma}_1 t}\exp\left(-\frac{t}{\bar{\gamma}_r}\right)\left[\mathrm{K}_1\left(2\sqrt{\frac{1}{\bar{\gamma}_1}\frac{\phi/G^2}{t}}\right)\right]^2\mathrm{d}t. \tag{6.29}$$

Applying [45, 11], [44, 03.04.26.0014.01], [36, 9.31-5], [36, 9.31-1], [36, 9.31-2] and finally [45, 21] in (6.29), the closed-form solution of I_2 is obtained as

$$I_2 = \frac{\sqrt{\pi}}{2} \exp\left(-\frac{\phi}{\bar{\gamma}_r}\right) G_{6,3}^{2,4}\left(\frac{\bar{\gamma}_1 \bar{\gamma}_r}{4\phi/G^2}\middle|\begin{matrix}0,1,-1,0,-1,-1\\ -1,-1,-\frac{1}{2}\end{matrix}\right). \tag{6.30}$$

Finally, the exact outage probability analysis for near user is obtained by substituting (6.27) and (6.30) in (6.23).

6.2.1.2 Outage probability of U_2

The outage probability of U_2 occurs when the received SNR at node U_2 is smaller than the target data rate. Then, the outage probability is defined as

$$P_{out}^2 = \Pr\{\gamma_2 \leq \gamma_{th_2}\}. \tag{6.31}$$

Substituting (6.11) in (6.31), we have

$$\begin{aligned} P_{out}^2 =& \Pr\left\{\frac{G^2|h_2|^2|h_r|^2 P_2}{G^2|h_2|^2|h_r|^2 P_1 + G^2|h_2|^2 N_0 + N_0} \leq \gamma_{th_2}\right\} \\ =& \Pr\left\{|h_2|^2 G^2\left(|h_r|^2\lambda - N_0\gamma_{th_2}\right) \leq N_0\gamma_{th_2}\right\} \end{aligned} \tag{6.32}$$

where $\lambda = P_2 - P_1\gamma_{th_2}$. The outage probability of U_2 in (6.32) is written as

$$P_{out}^2 = \Pr\left\{|h_r|^2 < \tau\right\} + \Pr\left\{|h_r|^2 > \tau,\, |h_2|^2 < \frac{\tau/G^2}{|h_r|^2 - \tau}\right\}. \tag{6.33}$$

Please note that for $\gamma_{th_2} > P_2/P_1$, P_{out}^2 is equal to one. Otherwise, (6.33) is expressed as

$$P_{out}^2 = \int_0^{\tau} p_{|h_r|^2}(y)\,\mathrm{d}y + \int_{\tau}^{\infty} p_{|h_r|^2}(y) F_{|h_2|^2}\left(\frac{\tau/G^2}{|h_r|^2 - \tau}\right)\mathrm{d}y. \tag{6.34}$$

Considering $M = 2$, $l = 1$, and $i = 2$ in (6.20), the ordered CDF of $|h_2|^2$ is expressed as

$$F_{|h_2|^2}(\gamma) = 2F_{|\tilde{h}_2|^2}(\gamma) - [F_{|\tilde{h}_2|^2}(\gamma)]^2. \tag{6.35}$$

Considering (6.19) and assuming $\chi = 2\sqrt{\frac{\gamma}{\bar{\gamma}_2}}\mathrm{K}_1\left(2\sqrt{\frac{\gamma}{\bar{\gamma}_2}}\right)$ where $\bar{\gamma}_2 = \Omega_2$, the ordered CDF of the far user in (6.35) is expressed as

$$\begin{aligned} F_{|h_2|^2}(\gamma) =& 2(1-\chi) - (1-\chi)^2 = 1 - \chi^2 \\ =& 1 - \omega_2(\gamma, \bar{\gamma}_2) \end{aligned} \tag{6.36}$$

where $\omega_2(\gamma, \bar{\gamma}_2)$ at the right hand side of (6.36) is defined as the function of γ and $\bar{\gamma}_2$. Finally, by substituting (6.36) in (6.34), P_{out}^2 is re-written as

$$P_{out}^2 = 1 - \underbrace{\int_{\tau}^{\infty} p_{|h_r|^2}(\gamma)\,\omega_2\left(\frac{\tau/G^2}{\gamma - \tau}, \bar{\gamma}_2\right)\mathrm{d}\gamma}_{I_3}. \tag{6.37}$$

Here, I_3 in (6.37) is similar to I_2 in (6.28) when we replace the parameters as $\phi \to \tau$. Following the same steps from (6.28) to (6.30) and assuming $\gamma - \tau = t$, the closed-form solution for P_{out}^2 in (6.37) is calculated as

$$P_{out}^2 = 1 - \frac{\sqrt{\pi}}{2} \exp\left(-\frac{\tau}{\bar{\gamma}_r}\right) G_{5,2}^{1,4}\left(\frac{\bar{\gamma}_2 \bar{\gamma}_r}{4\tau/G^2}\middle| \begin{matrix} 0,0,1,-1,0 \\ 0,-\frac{1}{2} \end{matrix}\right). \tag{6.38}$$

Finally, the overall outage probability of the proposed system is calculated as

$$P_{out} = 1 - (1 - P_{out}^1)(1 - P_{out}^2). \tag{6.39}$$

6.2.2 Ergodic capacity analysis

In this part, ergodic capacity of the considered cooperative AF relaying system using power domain NOMA-based technique under the condition of perfect SIC is investigated.

6.2.2.1 Ergodic capacity from the BS to U_1:

Ergodic capacity for near user by substituting (6.10) is shown as

$$E_{ave}^1 = E\left[\frac{1}{2}\log_2\left(1 + \frac{G^2|h_1|^2|h_r|^2 P_1}{G^2|h_1|^2 N_0 + N_0}\right)\right]. \tag{6.40}$$

For simplicity in calculation, we assume that $\theta = \frac{G^2|h_1|^2|h_r|^2 P_1}{G^2|h_1|^2 N_0 + N_0}$ and averaging (6.40) on θ with the simplifications is given as [27]

$$\begin{aligned} E_{ave}^1 &= \int_0^\infty \frac{1}{2}\log_2(1+\theta)\, p_\Theta(\theta)\, \mathrm{d}\theta \\ &= \frac{1}{2\ln 2}\int_0^\infty \frac{1 - F_\Theta(\theta)}{1+\theta}\, \mathrm{d}\theta. \end{aligned} \tag{6.41}$$

$F_\Theta(\theta)$ in (6.41) is calculated as

$$\begin{aligned} F_\Theta(\theta) &= \Pr\left\{\frac{G^2|h_1|^2|h_r|^2 P_1}{G^2|h_1|^2 N_0 + N_0} < \theta\right\} \\ &= \Pr\left\{|h_1|^2 G^2\left(|h_r|^2 P_1 - N_0\theta\right) < N_0\theta\right\}. \end{aligned} \tag{6.42}$$

After some simplification, (6.42) is written as

$$\begin{aligned} F_\Theta(\theta) &= \Pr\left\{|h_r|^2 > \frac{N_0\theta}{P_1}, |h_1|^2 < \frac{N_0\theta/G^2}{|h_r|^2 P_1 - N_0\theta}\right\} + \Pr\left\{|h_r|^2 < \frac{N_0\theta}{P_1}\right\} \\ &= \int_0^{\frac{N_0\theta}{P_1}} p_{|h_r|^2}(y)\, \mathrm{d}y + \int_{\frac{N_0\theta}{P_1}}^{\infty} p_{|h_r|^2}(y) F_{|h_1|^2}\left(\frac{N_0\theta/G^2}{yP_1 - N_0\theta}\right) \mathrm{d}y \end{aligned} \tag{6.43}$$

Substituting the ordered CDF for near user in (6.21) in (6.43), we have

$$F_{\Theta}(\theta) = 1 - \underbrace{\int_{\frac{N_0\theta}{P_1}}^{\infty} p_{|h_r|^2}(y)\, \omega_1\left(\frac{N_0\theta/G^2}{P_1 y - N_0\theta}, \bar{\gamma}_1\right) \mathrm{d}y}_{J_1} + \underbrace{\int_{\frac{N_0\theta}{P_1}}^{\infty} p_{|h_r|^2}(y)\, \omega_2\left(\frac{N_0\theta/G^2}{P_1 y - N_0\theta}, \bar{\gamma}_1\right) \mathrm{d}y}_{J_2} \tag{6.44}$$

Furthermore, substituting (6.18) and (6.22a) in the second term of the right hand side of (6.44), J_1 is obtained as

$$J_1 = \int_{\frac{N_0\theta}{P_1}}^{\infty} \frac{1}{\bar{\gamma}_r} exp\left(-\frac{y}{\bar{\gamma}_r}\right) 4\sqrt{\frac{1}{\bar{\gamma}_1}\frac{N_0\theta/G^2}{P_1 y - N_0\theta}}\mathrm{K}_1\left(4\sqrt{\frac{1}{\bar{\gamma}_1}\frac{N_0\theta/G^2}{P_1 y - N_0\theta}}\right) \mathrm{d}y \tag{6.45}$$

where we have assume that $yP_1 - N_0\theta = t$. Thus, we have

$$J_1 = \kappa_2 \sqrt{\frac{N_0\theta/G^2}{\bar{\gamma}_1}} \int_0^{\infty} t^{-1/2} \exp\left(-\frac{t}{\bar{\gamma}_r P_1}\right) \mathrm{K}_1\left(2\sqrt{\frac{1}{\bar{\gamma}_1}\frac{N_0\theta/G^2}{t}}\right) \mathrm{d}t \tag{6.46}$$

where $\kappa_2 = \frac{4}{\bar{\gamma}_r P_1} \exp\left(-\frac{N_0\theta}{\bar{\gamma}_r P_1}\right)$ and using [45, 11], [36, 9.31-1], [45, 14], [36, 9.31-2] and [36, 9.31-5], (6.46) can be re-expressed as

$$J_1 = 2\exp\left(-\frac{N_0\theta}{\bar{\gamma}_r P_1}\right) G_{2,5}^{3,2}\left(\frac{N_0\theta/G^2}{\bar{\gamma}_r\bar{\gamma}_1 P_1}\middle| \begin{matrix} 2, \frac{3}{2} \\ 1,1,0,\frac{3}{2},2 \end{matrix}\right). \tag{6.47}$$

Furthermore, J_2 term in (6.44) is obtained by substituting (6.18) and (6.22b) and is calculated as

$$J_2 = \kappa_2 \frac{N_0\theta/G^2}{\bar{\gamma}_1} \int_0^{\infty} t^{-1} \exp\left(-\frac{t}{\bar{\gamma}_r P_1}\right) \left[\mathrm{K}_1\left(2\sqrt{\frac{1}{\bar{\gamma}_1}\frac{N_0\theta/G^2}{t}}\right)\right]^2 \mathrm{d}t. \tag{6.48}$$

Then, applying [44, 03.04.26.0014.01], [36, 9.31-5], [36, 9.31-1], [36, 9.31-2] and [36, 7.813-1] respectively, we obtain

$$J_2 = \frac{\sqrt{\pi}}{2} \exp\left(-\frac{N_0\theta}{\bar{\gamma}_r P_1}\right) G_{5,2}^{1,4}\left(\frac{\bar{\gamma}_1\bar{\gamma}_r P_1}{4N_0\theta/G^2}\middle| \begin{matrix} 0,0,1,-1,0 \\ 0,-\frac{1}{2} \end{matrix}\right). \tag{6.49}$$

Moreover, by substituting (6.44) in (6.41), the ergodic capacity for the near user is given as

$$E_{ave}^1 = \frac{1}{2\ln 2}\int_0^{\infty} \frac{J_1 - J_2}{1+\theta}\,\mathrm{d}\theta = \frac{1}{2\ln 2}\left[\mathscr{M}_1 - \mathscr{M}_2\right] \tag{6.50}$$

where $\mathscr{M}_1 = \int_0^\infty \frac{J_1}{1+\theta}\,\mathrm{d}\theta$ and $\mathscr{M}_2 = \int_0^\infty \frac{J_2}{1+\theta}\,\mathrm{d}\theta$. Here, $\mathscr{M}_1$ and $\mathscr{M}_2$ are given as

$$\mathscr{M}_1 = 2\int_0^\infty \frac{1}{1+\theta}\exp\left(-\frac{N_0\theta}{\bar{\gamma}_r P_1}\right) G_{2,5}^{3,2}\left(\frac{N_0\theta/G^2}{\bar{\gamma}_r\bar{\gamma}_1 P_1}\middle|\begin{matrix}2,\frac{3}{2}\\ 1,1,0,\frac{3}{2},2\end{matrix}\right)\mathrm{d}\theta \tag{6.51}$$

and

$$\mathscr{M}_2 = \frac{\sqrt{\pi}}{2}\int_0^\infty \frac{1}{1+\theta}\exp\left(-\frac{N_0\theta}{\bar{\gamma}_r P_1}\right) G_{5,2}^{1,4}\left(\frac{\bar{\gamma}_1\bar{\gamma}_r P_1}{4N_0\theta/G^2}\middle|\begin{matrix}0,0,1,-1,0\\ 0,-\frac{1}{2}\end{matrix}\right)\mathrm{d}\theta \tag{6.52}$$

respectively. Using [45, 10], [45, 11] and [44, 07.34.21.0081.01], $\mathscr{M}_1$ is obtained as (6.51) can be expressed as

$$\mathscr{M}_1 = 2\,G_{1,1:0,1:2,5}^{1,1:1,0:3,2}\left(\frac{N_0}{\bar{\gamma}_r P_1}, \frac{N_0/G^2}{\bar{\gamma}_r\bar{\gamma}_1 P_1}\middle|\begin{matrix}0\\ 0\end{matrix}\middle|-\middle|\begin{matrix}2,\frac{3}{2}\\ 1,1,0,\frac{3}{2},2\end{matrix}\right) \tag{6.53}$$

where $G_{p,q:p_1,q_1:p_2,q_2}^{m,n:m_1,n_1:m_2,n_2}(.,.|:|:|:)$ is the extended generalized bi-variate Meijer's G function [44]. Moreover, by following the similar steps and [36, 9.31-2], $\mathscr{M}_2$ is written as

$$\mathscr{M}_2 = \frac{\sqrt{\pi}}{2}\,G_{1,1:0,1:2,5}^{1,1:1,0:4,1}\left(\frac{N_0}{\bar{\gamma}_r P_1}, \frac{4N_0/G^2}{\bar{\gamma}_r\bar{\gamma}_1 P_1}\middle|\begin{matrix}0\\ 0\end{matrix}\middle|-\middle|\begin{matrix}1,\frac{3}{2}\\ 1,1,0,2,1\end{matrix}\right). \tag{6.54}$$

Finally, by substituting (6.53) and (6.54) in (6.50), the E_{ave}^1 for the near user U_1 is obtained in the closed-form. Please note that, there is no built-in function for bi-variate Meijer's G function. Therefore, the results are evaluated numerically using (6.51) and (6.52).

6.2.2.2 Ergodic capacity from the BS to U_2:

The ergodic capacity for far user U_2 considering (6.11) is given as

$$E_{ave}^2 = E\left[\frac{1}{2}\log_2\left(1+\frac{G^2|h_2|^2|h_r|^2P_2}{G^2|h_2|^2|h_r|^2P_1+G^2|h_2|^2N_0+N_0}\right)\right]. \tag{6.55}$$

For simplicity in calculation, we assume that $\xi = \frac{G^2|h_2|^2|h_r|^2P_2}{G^2|h_2|^2|h_r|^2P_1+G^2|h_2|^2N_0+N_0}$. Moreover, (6.55) is calculated as

$$E_{ave}^2 = \int_0^\infty \frac{1}{2}\log_2(1+\xi)\,p_\Xi(\xi)\,\mathrm{d}\xi = \frac{1}{2\ln 2}\int_0^\infty \frac{1-F_\Xi(\xi)}{1+\xi}\,\mathrm{d}\xi \tag{6.56}$$

where $F_\Xi(\xi)$ is defined as

$$\begin{aligned} F_\Xi(\xi) &= \Pr\left\{\frac{G^2|h_2|^2|h_r|^2P_2}{G^2|h_2|^2|h_r|^2P_1+G^2|h_2|^2N_0+N_0} < \xi\right\} \\ &= \Pr\left\{|h_1|^2G^2\left(|h_r|^2P_2 - |h_r|^2P_1\xi - N_0\xi\right) < N_0\xi\right\}. \end{aligned} \tag{6.57}$$

After performing some mathematical simplification, (6.57) is re-written as

$$F_{\Xi}(\xi) = \Pr\left\{ |h_r|^2 > \frac{N_0\xi}{P_2 - P_1\xi}, |h_2|^2 < \frac{N_0\xi/G^2}{|h_r|^2(P_2 - P_1\xi) - N_0\xi} \right\} + \Pr\left\{ |h_r|^2 < \frac{N_0\xi}{P_2 - P_1\xi} \right\}. \tag{6.58}$$

In (6.58), assuming $\xi < P_2/P_1$, the $F_{\Xi}(\xi)$ is calculated as

$$F_{\Xi}(\xi) = \int_0^{\frac{N_0\xi}{\beta}} p_{|h_r|^2}(y)\,\mathrm{d}y + \int_{\frac{N_0\xi}{\beta}}^{\infty} p_{|h_r|^2}(y) F_{|h_2|^2}\left(\frac{N_0\xi/G^2}{y\beta - N_0\xi}\right)\mathrm{d}y \tag{6.59}$$

where $\beta = P_2 - P_1\xi$. Using the ordered CDF for far user given in (6.36) and after substituting it in (6.59) we have

$$F_{\Xi}(\xi) = 1 - \underbrace{\int_{\frac{N_0\xi}{\beta}}^{\infty} p_{|h_r|^2}(y)\,\omega_2\left(\left.\frac{N_0\xi/G^2}{\beta y - N_0\xi}\right|_{\bar{\gamma}_1 \to \bar{\gamma}_2}\right)\mathrm{d}\gamma}_{J_3}. \tag{6.60}$$

Here, considering the third term of (6.44), substituting $J_2 = J_3(\bar{\gamma}_1 \to \bar{\gamma}_2)$, and under the assumption $\xi < P_2/P_1$ as in (6.58), the expression in (6.60) is defined as $F_{\Xi}(\xi) = 1 - J_3$. Furthermore, substituting (6.60) in (6.56), E^2_{ave} is re-written as

$$E^2_{ave} = \frac{1}{2\ln 2}\int_0^{\frac{P_2}{P_1}} \frac{J_3}{1+\xi}\,\mathrm{d}\xi. \tag{6.61}$$

where

$$J_3 = J_2\Big|_{P_1 \to \beta} = \frac{\sqrt{\pi}}{2}\exp\left(-\frac{N_0\xi}{\bar{\gamma}_r\beta}\right) G^{1,4}_{5,2}\left(\frac{\bar{\gamma}_2\bar{\gamma}_r\beta}{4N_0\xi/G^2}\middle|\begin{matrix}0,0,1,-1,0\\ 0,-\frac{1}{2}\end{matrix}\right). \tag{6.62}$$

Finally, the ergodic capacity at far user is calculated as

$$E^2_{ave} = \frac{1}{2\ln 2}\frac{\sqrt{\pi}}{2}\int_0^{\frac{P_2}{P_1}} \frac{1}{1+\xi}\exp\left(-\frac{N_0\xi}{\bar{\gamma}_r\beta}\right) G^{1,4}_{5,2}\left(\frac{\bar{\gamma}_2\bar{\gamma}_r\beta}{4N_0\xi/G^2}\middle|\begin{matrix}0,0,1,-1,0\\ 0,-\frac{1}{2}\end{matrix}\right)\mathrm{d}\xi. \tag{6.63}$$

Since (6.63) is not analytically tractable, the closed-form solution of E^2_{ave} is obtained numerically.

Finally, ergodic sum rate analysis for overall system is given as

$$E_{ave} = E^1_{ave} + E^2_{ave}. \tag{6.64}$$

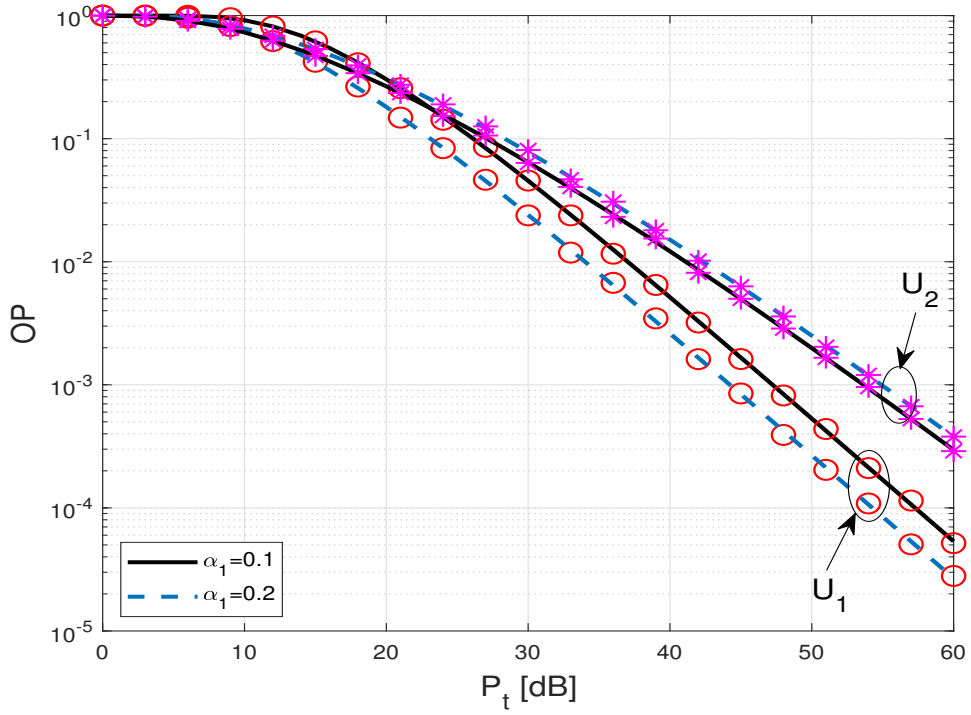

Figure 6.2 : Outage performance analysis of users in different power allocations when $R_1 = 0.5$, $R_2 = 0.5$ and $d_{sr} = 0.5$, $d_1 = 0.5$, $d_2 = 0.7$.

6.2.3 Performance analysis

In this section, the proposed theoretical and simulation results are provided for outage probability and ergodic capacity. Moreover, BS, R, and both users are assumed to be located co-linearly. Unless otherwise stated, we assume that the noise variance at each node is assumed equally as $N_0 = 1$ and the channel gains are given as $\Omega_{sr} = 1/(1+d_{sr}^2)$, $\Omega_1 = 1/(1+d_1^2)$, and $\Omega_2 = 1/(1+d_2^2)$. The analytical results and Monte-Carlo simulations are presented and verified together. Markers represent the simulation results, whereas lines represent theoretical analysis in all figures.

Fig. 6.2 denotes P_t versus the outage probability analysis of both users. Here, it is assumed that the target data rates are assigned as $R_1 = R_2 = 0.5$. Furthermore, the normalized distances are assumed as $d_{sr} = 0.5$, $d_1 = 0.5$ and $d_2 = 0.7$. The results are obtained for different power allocation coefficients. As shown in Fig. 6.2, when the value of α_1 is increased from 0.1 to 0.2, since U $_1$ is the user with strong channel conditions, it has about 3 dB of SNR gain. However, for U_2, α_2 is decreased from 0.9 to 0.8. Since the power allocation is decreased about 11%, we have an about 1.5

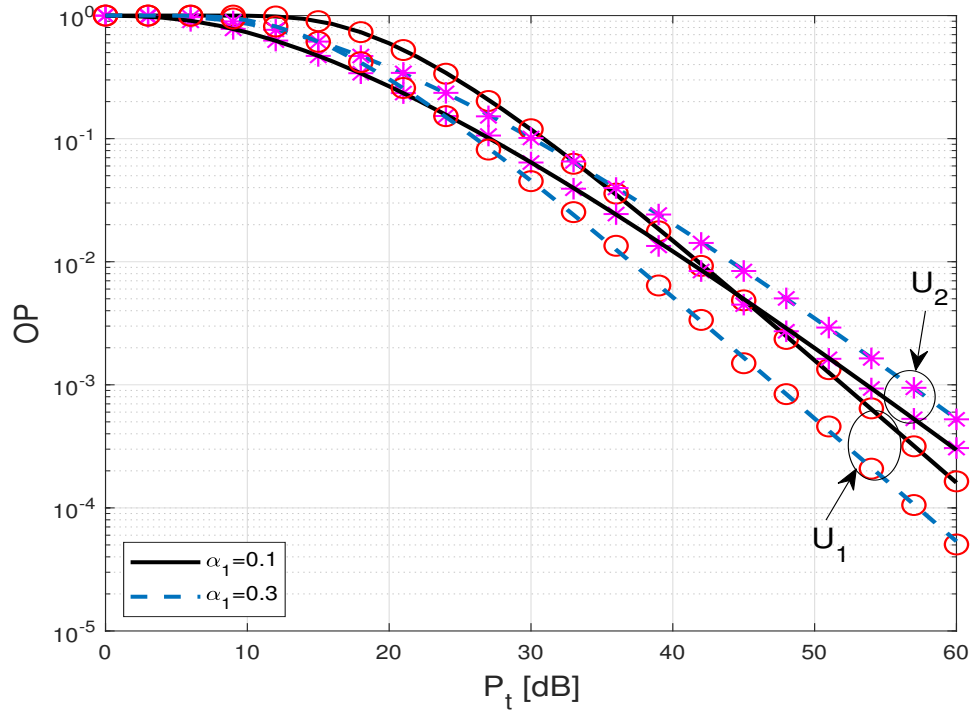

Figure 6.3 : Outage performance analysis of users in different power allocations when $R_1 = 1$, $R_2 = 0.5$ and $d_{sr} = 0.5$, $d_1 = 0.5$, $d_2 = 0.7$.

dB SNR loss. Moreover, for a fixed value of α_1, U_1 performs better compared to U_2 mostly at middle and high SNR values.

Fig. 6.3 shows P_t versus the outage probability of both users. The results are provided, assuming that distances are the same as in Fig. 6.2. It is assumed that the target data rates are assigned as $R_1 = 1$ and $R_2 = 0.5$. Here, we set the corresponding target data rate as $R_2 = 0.5$ for the far user U_2 so that the performance of U_2 is compensated in the large distance by taking a small rate. Considering the provided results of U_1 in Fig. 6.2 when $\alpha_1 = 0.1$ and in Fig. 6.3 when $\alpha_1 = 0.3$, we can say that they have nearly the same performance. So, U_1 can send one more data bit to have the same outage probability by taking a large power allocation. Moreover, the results show that with the increase of power allocation, the performance of U_1 is increasing and performance of U_2 decreases. Additionally, the performance of U_2 is better compared to U_1 for a fixed value of $\alpha_1 = 0.1$ at low and middle SNR. This is because power allocation for U_1 is substantially low due to the high order modulation.

In Fig. 6.4, the outage probability analysis of both users and overall system performance according to different power allocation parameters for $P_t = 45$ dB is investigated. The normalized distances are assumed as $d_{sr} = 0.5$, $d_1 = 0.5$ and $d_2 = 0.8$.

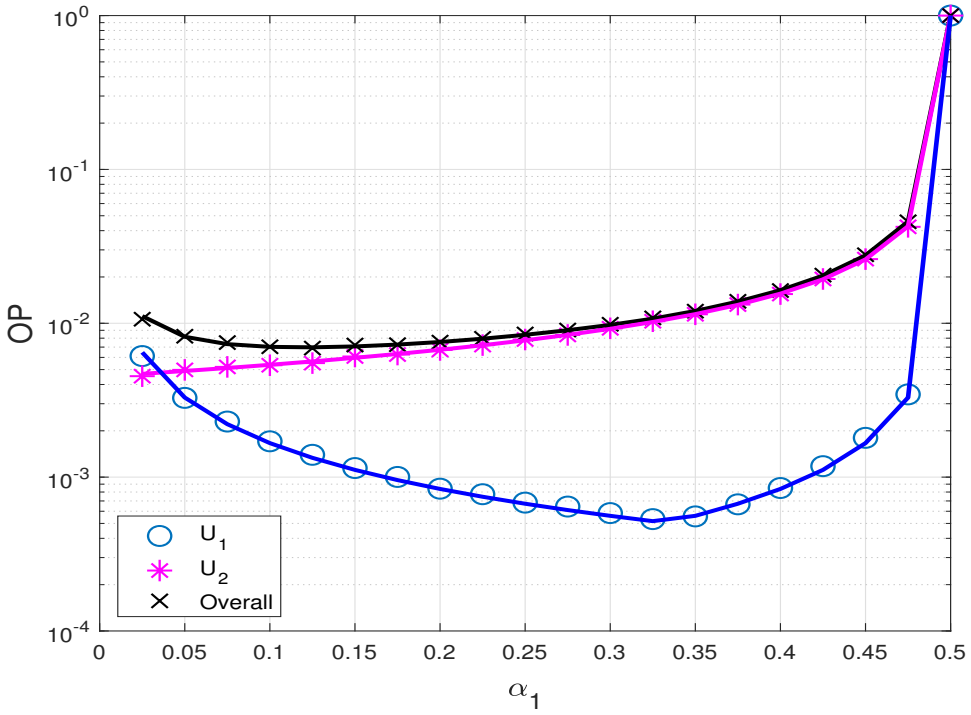

Figure 6.4 : Outage performance analysis of users and overall when $R_1 = 0.5$, $R_2 = 0.5$ and $d_{sr} = 0.5$, $d_1 = 0.5$, $d_2 = 0.8$.

Besides, the target data rates are assigned as $R_1 = R_2 = 0.5$. Here, the overall system performance and the performance of U_2 converge when $0.32 \leq \alpha_1 < 0.5$. The optimum power allocation coefficient for U_1 corresponds to the convergence point of U_2 and overall system performance when $\alpha_1 = 0.32$. Besides, increasing the power allocation $\alpha_1 > 0.32$ causes the performance decrease for U_1. The reason is U_1 cannot perform better since U_2 can not be decoded correctly, which causes the failure of SIC procedure. Also, increasing the power allocation coefficient more than $\alpha_1 = 0.5$, the criteria of $\gamma_{th_2} < P_2/P_1$ cannot be met and the outage performance goes to one.

Fig. 6.5 presents both users and overall system performance in terms of outage probability with increasing distance when $P_t = 50$ dB and $\alpha_1 = 0.2$. The target data rates are assumed as $R_1 = 1$, $R_2 = 0.5$. Here, the coverage distance for BS is assigned as $d = 5$ m, and both users are assumed to be at equal distance to R under the condition of $d_1 = d_2 = d - d_{sr}$. When $d_{sr} = 4$ m, users are achieved the same outage performance, which means user fairness is reached. Furthermore, when $d_{sr} = 4.5$ m, the total system performance reaches its highest value. The performance of U_1 deteriorates while $d_{sr} \geq 3.7$ due to the failure of the SIC procedure.

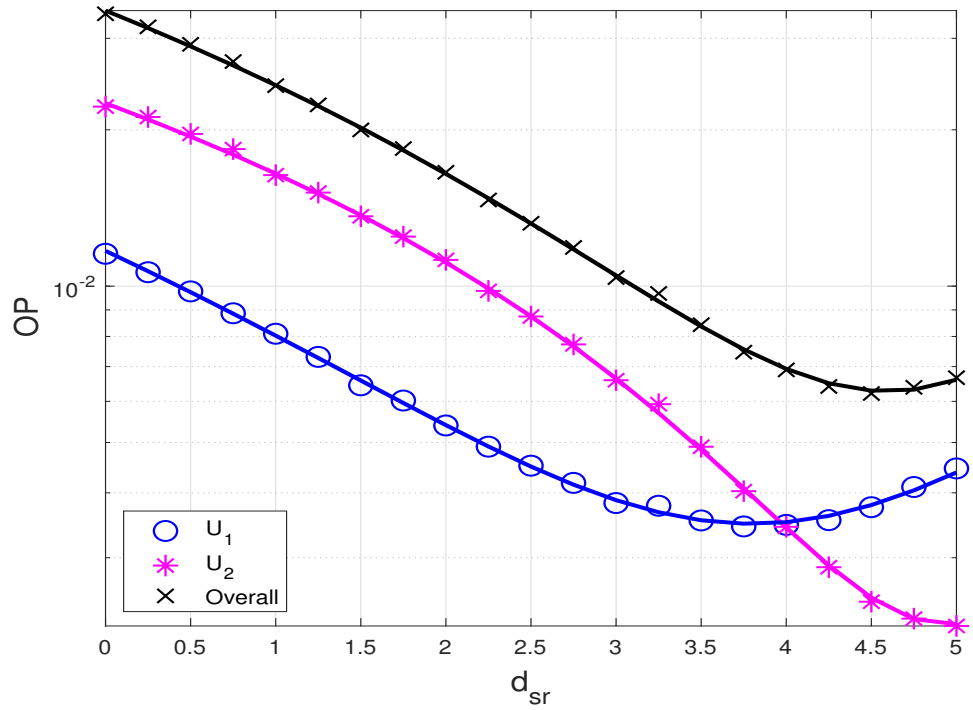

Figure 6.5 : Outage performance analysis of both users and the overall system when $R_1 = 1$, $R_2 = 0.5$, $P_t = 50$ dB and $\alpha_1 = 0.2$.

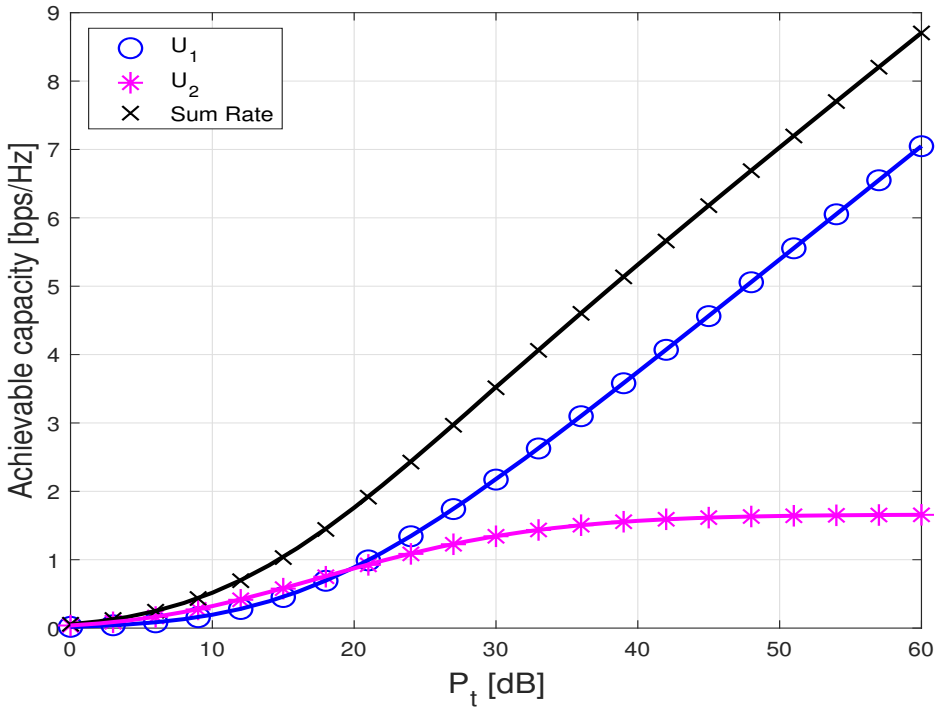

Figure 6.6 : Ergodic capacity of both users and the overall system when $d_{sr} = 0.5$, $d_1 = 0.5$, $d_2 = 0.8$ and $\alpha_1 = 0.1$.

Fig. 6.6 displays the ergodic capacity analysis for both users and the overall system versus transmission power of the BS. The power allocation coefficient is $\alpha_1 = 0.1$ and the normalized distances are assigned as $d_{sr} = 0.5$, $d_1 = 0.5$, $d_2 = 0.8$. Here, the

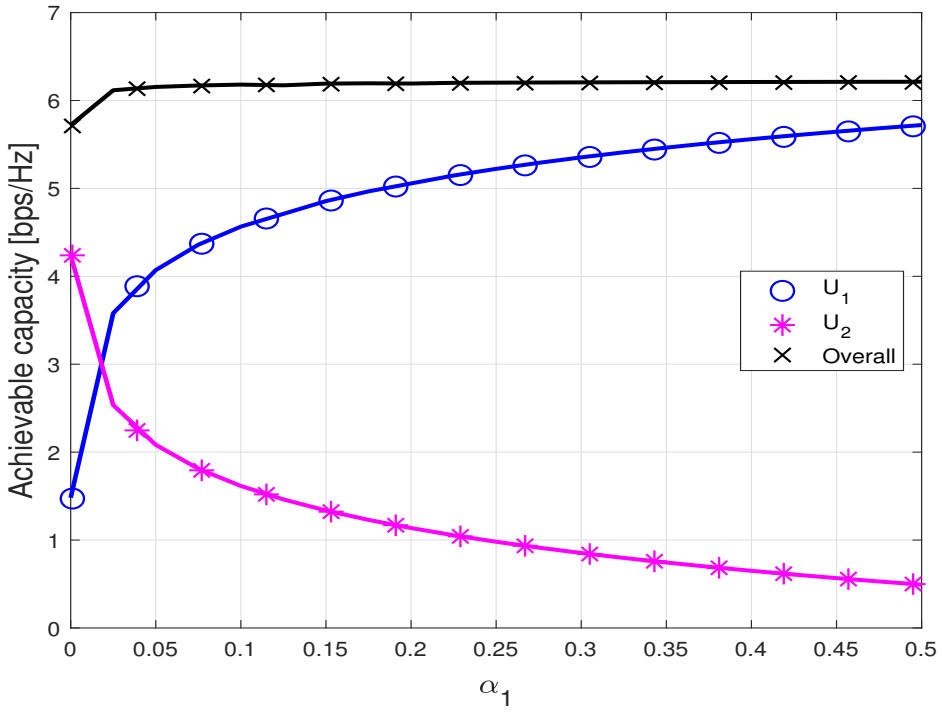

Figure 6.7 : Ergodic capacity of both users and the overall system when $d_{sr} = 0.5$, $d_1 = 0.5$, $d_2 = 0.8$ and $P_t = 45$ dB.

ergodic capacity of U_2 is saturated at high SNR values due to the interference from the U_1 and low quality of channel conditions. Nevertheless, since U_1 successfully decodes its information without interference from U_2, increased transmission power improves the achiaveble capacity at U_1 and overall system performance.

Fig. 6.7 presents the ergodic capacity performance for both users and the overall system versus power allocation parameter. It is assumed that $P_t = 45$ dB and the normalized distances are $d_{sr} = 0.5$, $d_1 = 0.5$ and $d_2 = 0.8$. It is shown in Fig. 6.7 that, since $\alpha_1 + \alpha_2 = 1$, increasing α_1 results in a better achievable rate at U_1 while a decrease in the achievable rate at U_2. However, the total ergodic rate for this system saturates to about 6 bps/Hz even at small power allocation values.

In this chapter, the effect of NOMA techniques in a cooperative vehicular environment is investigated where the inter-vehicle channels are exposed to cascade fading. The theoretical expressions of outage probability and ergodic capacity are derived and Monte-Carlo simulations verify the analytical results.

7. CONCLUSIONS

In this thesis, the error performance of a vehicular communication system has been studied when the relay applies DF and AF relaying protocols over double Rayleigh fading channels. The relay is assumed to have more than one antenna and applies the MRC technique on the receiver side, providing diversity and increasing system performance. The results have been shown that both DF and AF relaying protocols provide similar performances at high and medium SNR values. However, at low SNR values, DF relaying protocol override compared to AF relaying protocol. Please note that the noise is transmitted along with the received signal at the relay in AF relaying protocol, unlike DF relaying. The simulation results are also consistent with the lower bound theoretical derivations for both considered relaying protocols.

Furthermore, PLS performance has been considered for V2V cooperative communication systems where the source transmits the signal to the destination node through the relay applying the DF relaying protocol. On the other hand, it is assumed that E listens to both source and relay with multiple antennas and applies the MRC technique. Since all the nodes are mobile, the channels between them are assumed as double Rayleigh fading. The numerical and simulation results have been shown that increasing the number of E antennas significantly decreases secrecy outage performance. It is also determined that as the average received SNR for both links S$\rightarrow$E and R$\rightarrow$E increases, the overall system secrecy capacity gets weaker. Moreover, in addition to SOP analysis, PPSC analysis has also been calculated using SOP expression. The computer simulation results have been verified by theoretical derivations.

Additionally, the power domain downlink NOMA-based dual-hop system is studied while R applies the fixed-gain AF relaying protocol for vehicular communications. Considering the perfect SIC conditions, the inter-vehicle channels are assumed to have double Rayleigh fading. However, the channel between BS and R is subject to Rayleigh fading. The overall system and performance of users are analyzed in terms of outage probability and ergodic capacity. Moreover, the results have been analyzed

considering transmission power, power allocation coefficient, and distance parameters, as well as outage probability and ergodic capacity. Monte-Carlo simulation results have been validated with analytical closed-form derivations.

REFERENCES

[1] **Wu, G.**, **Xu, P.**, **Zhu, W. and Bui, T.** (2016). Relay-Assisted Based AF in Two-Hop Vehicular Networks over Rayleigh Fading Channels, *2016 IEEE 83rd Vehicular Tech. Conf.*, pp.1–4.

[2] **Bithas, P.S.**, **Efthymoglou, G.P. and Kanatas, A.G.** (2018). V2V Cooperative Relaying Communications Under Interference and Outdated CSI, *IEEE Trans. on Vehicular Tech.*, *67*(4), 3466–3480.

[3] **Feteiha, M.F. and Ahmed, M.H.** (2018). Multihop Best-Relay Selection for Vehicular Communication Over Highways Traffic, *IEEE Trans. on Vehicular Tech.*, *67*(10), 9845–9855.

[4] **Ata, S.O. and Altunbas, I.** (2015). Relay Antenna Selection for V2V Communications Using PLNC over Cascaded Fading Channels, *IEEE Proc. Int. Wireless Comm. and Mobile Computing Conf. (IWCMC)*.

[5] **Alghorani, Y. and et al** (2016). On the Performance of Multihop-Intervehicular Communications Systems Over N*Rayleigh Fading Channels, *IEEE Wireless Comm. Letters*, *5*(2), 116–119.

[6] **Hajri, N.**, **Khedhiri, R. and Youssef, N.** (2020). On Selection Combining Diversity in Dual-Hop Relaying Systems over Double Rice Channels: Fade Statistics and Performance Analysis, *IEEE Access*, *8*, 72188–72203.

[7] **Kosu, S.**, **Ata, S.O. and Durak-Ata, L.** (2019). On the Error Performance of Relay-Assisted Vehicular Communication Systems, *Proc. 2019 IEEE Microwave Theory and Techniques in Wireless Comm., MTTW 2019*, pp.68–71.

[8] **Dong Qin, Yuhao Wang, T.Z.** (2020). Performance Analysis of Bidirectional AF Based Cooperative Vehicular Networks, *IEEE Trans. on Vehicular Tech.*, *69*(2), 2274–2279.

[9] **Moualeu, J.M.**, **da Costa, D.B.**, **Lopez-Martinez, F.J.**, **Hamouda, W.**, **Ngatched, T.M.N. and Dias, U.S.** (2019). Secrecy Analysis of a TAS/MRC Scheme in $\alpha - \mu$ Fading Channels, *IEEE Wireless Comm. and Net. Conf. (WCNC)*, pp.1–6.

[10] **Li, T.**, **Zhang, T.**, **Zhong, B.**, **Zhang, Z. and Vasilakos, A.V.** (2015). Physical Layer Security via Maximal Ratio Combining and Relay Selection over Rayleigh Fading Channel, *IEEE 26th Int. Symp. on Personal, Indoor, and Mobile Radio Comm. (PIMRC)*, pp.612–616.

[11] **Chen, G.**, **Gong, Y.**, **Xiao, P. and Chambers, J.A.** (2015). Physical Layer Network Security in the Full-Duplex Relay System, *IEEE Trans. Information Forensics and Security*, *10*(3), 574–583.

[12] **Ata, S.Ö.** (2018). Secrecy Performance Analysis Over Double Nakagami-*m* Fading Channels, *Proc. 2018 41st International Conf. on Telecommunications and Signal Processing (TSP)*, pp.1–4.

[13] **Ata, S.Ö.** (2018). Secrecy Performance Analysis Over Cascaded Nakagami-*m* Fading Channels, *IET Comm.*, volume 13, pp.259–265.

[14] **Kong, L.**, **Kaddoum, G. and da Costa, D.B.** (2018). Cascaded $\alpha - \mu$ Fading Channels: Reliability and Security Analysis, *IEEE Access*, *6*, 41978–41992.

[15] **Kong, L.**, **Ai, Y.**, **He, J.**, **Rajatheva, N. and Kaddoum, G.** (2019). Intercept Probability Analysis over the Cascaded Fisher-Snedecor Fading Channels, *IEEE 16th Int. Symp. Wireless Comm. Sys.*, p.672–676.

[16] **Pandey, A. and Yadav, S.** (2018). Physical Layer Security in Cooperative AF Relaying Networks With Direct Links Over Mixed Rayleigh and Double-Rayleigh Fading Channels, *IEEE Trans. Vehic. Tech.*, *67*(11), 10615–10630.

[17] **Zhang, J. and Pan, G.** (2017). Secrecy Outage Analysis with Kth Best Relay Selection in Dual-Hop Inter-Vehicle Communication Systems, *AEU - Int. Journal of Elect. and Comm.*, *71*, 139 – 144.

[18] **Alsmadi, M.M.**, **Ali, N.A.**, **Hayajneh, M. and Ikki, S.S.** (2020). Downlink NOMA Networks in the Presence of IQI and Imperfect SIC: Receiver Design and Performance Analysis, *IEEE Trans. on Vehicular Tech.*, *69*(6), 6793–6797.

[19] **Sadia, H.**, **Zeeshan, M. and Sheikh, S.A.** (2018). Performance Analysis of Downlink Power Domain NOMA under Fading Channels, *Proc. 12th International Conf. ELEKTRO 2018, 2018 ELEKTRO Conf. Proceedings*, IEEE, pp.1–6.

[20] **Zhu, L.**, **Zhang, J.**, **Xiao, Z.**, **Cao, X. and Wu, D.O.** (2019). Optimal User Pairing for Downlink Non-orthogonal Multiple Access (NOMA), *IEEE Wireless Comm. Letters*, *8*(2), 328–331.

[21] **Liau, Q.Y. and Leow, C.Y.** (2019). Successive User Relaying in Cooperative NOMA System, *IEEE Wireless Comm. Letters*, *8*(3), 921–924.

[22] **Soni, B.**, **Patel, D.K.**, **Guan, Y.L.**, **Sun, S.**, **Chang, Y.C. and Lim, J.M.Y.** (2020). Performance Analysis of NOMA Aided Cooperative Relaying over α-η-κ-μ Fading Channels, *Proc. 26th National Conf. on Comm., NCC*, IEEE.

[23] **Kara, F. and Kaya, H.** (2019). On the Error Performance of Cooperative-NOMA with Statistical CSIT, *IEEE Comm. Letters*, *23*(1), 128–131.

[24] **Men, J. and Ge, J.** (2015). Performance Analysis of Non-orthogonal Multiple Access in Downlink Cooperative Network, *IET Comm.*, *9*(18), 2267–2273.

[25] **Aldababsa, M. and Kucur, O.** (2020). Performance of Cooperative Multiple-input Multiple-output NOMA in Nakagami-*m* Fading Channels with Channel Estimation Errors, *IET Comm.*, *14*(2), 274–281.

[26] **Men, J.**, **Ge, J. and Zhang, C.** (2017). Performance Analysis for Downlink Relaying Aided Non-orthogonal Multiple Access Networks with Imperfect CSI over Nakagami- *m* fading, *IEEE Access*, *5*, 998–1004.

[27] **Men, J.**, **Ge, J. and Zhang, C.** (2017). Performance Analysis of Nonorthogonal Multiple Access for Relaying Networks over Nakagami-*m* Fading Channels, *IEEE Trans. on Vehicular Tech.*, *66*(2), 1200–1208.

[28] **Abbasi, O.**, **Ebrahimi, A. and Mokari, N.** (2019). NOMA Inspired Cooperative Relaying System Using an AF Relay, *IEEE Wireless Comm. Letters*, *8*(1), 261–264.

[29] **Joshi, S. and Mallik, R.K.** (2019). Cooperative NOMA with AF Relaying over Nakagami-*m* Fading in a D2D Network, *Proc. IEEE Vehicular Tech. Conf.*, volume2019-April, IEEE.

[30] **Di, B.**, **Song, L.**, **Li, Y. and Han, Z.** (2017). V2X Meets NOMA: Non-orthogonal Multiple Access for 5G-enabled Vehicular Networks, *IEEE Wireless Comm.*, *24*(6), 14–21.

[31] **Jaiswal, N. and Purohit, N.** (2019). Performance Evaluation of Non-orthogonal Multiple Access in V2V Communications over Double-Rayleigh Fading Channels, *Proc. 2019 IEEE Conf. on Information and Communication Tech., CICT 2019*, IEEE, pp.0–4.

[32] **Gurugopinath, S.**, **Sofotasios, P.C.**, **Al-Hammadi, Y. and Muhaidat, S.** (2019). Cache-aided Non-orthogonal Multiple Access for 5G-enabled Vehicular Networks, *IEEE Trans. on Vehicular Tech.*, *68*(9), 8359–8371.

[33] **Matolak, D.W. and Frolik, J.** (2011). Worse-than-Rayleigh Fading: Experimental Results and Theoretical Models, *IEEE Comm. Magazine*, *49*(4), 140–146.

[34] **Simon, M.K. and Alouini, M.S.** (2005). *Digital Communication over Fading Channels; 2nd ed.*, Wiley, Newark, NJ.

[35] **Duy, T.T.**, **Alexandropoulos, G.C.**, **Tung, V.T.**, **Son, V.N. and Duong, T.Q.** (2016). Outage Performance of Cognitive Cooperative Networks with Relay Selection over Double-Rayleigh Fading Channels, *IET Comm.*, *10*(1), 57–64.

[36] **Gradshteyn, I.S. and Ryzhik, I.M.** (2007). *Table of Integrals, Series, and Products*, 7th ed., MA, USA: Elsevier.

[37] **Salo, J.**, **El-Sallabi, H.M. and Vainikainen, P.** (2006). The Distribution of the Product of Independent Rayleigh Random Variables, *IEEE Trans. on Antennas and Propagation*, *54*(2), 639–643.

[38] **Chatzidiamantis, N.D. and Karagiannidis, G.K.** (2011). On the Distribution of the Sum of Gamma-Gamma Variates and Applications in RF and Optical Wireless Comm., *IEEE Trans. on Comm.*, *59*(5), 1298–1308.

[39] **Rappaport, T.** (2001). *Wireless Communications: Principles and Practice*, Prentice Hall PTR, USA, 2nd edition.

[40] **Ikki, S. and Ahmed, M.H.** (2007). Performance Analysis of Cooperative Diversity Wireless Networks over Nakagami-*m* Fading Channel, *IEEE Commun. Lett.*, *11*(4), 334–336.

[41] **Papoulis, A. and Pillai, S.** (2002). *Probability, Random Variables, and Stochastic Processes*, McGraw-Hill.

[42] **Louie, R.H.Y.**, **Li, Y. and Vucetic, B.** (2010). Practical Physical Layer Network Coding for Two-way Relay Channels: Performance Analysis and Comparison, *IEEE Trans. on Wireless Commun.*, *9*(2), 764–777.

[43] **Proakis, J.G.** (1995). *Digital Communications*, McGraw-Hill.

[44] **Wolfram Inc.**, (2018), The mathematical functions site, `http://functions.wolfram.com`, [Online].

[45] **Adamchik, V.S. and Marichev, O.I.** (1990). The Algorithm for Calculating Integrals of Hypergeometric Type Functions and Its Realization in REDUCE System, *Proc. Int. Symp. on Symbolic and Algebraic Comput.*, ISSAC '90, pp.212–224.

[46] **Hasna, M.O. and Alouini, M.S.** (2004). Harmonic Mean and End-to-End Performance of Transmission Systems with Relays, *IEEE Trans. on Commun.*, *52*(1), 130–135.

[47] **Zhang, J.**, **Li, G.**, **Marshall, A.**, **Hu, A. and Hanzo, L.** (2020). A New Frontier for IoT Security Emerging From Three Decades of Key Generation Relying on Wireless Channels, *IEEE Access*, *8*, 138406–138446.

[48] **Zou, Y.**, **Zhu, J.**, **Wang, X. and Hanzo, L.** (2016). A Survey on Wireless Security: Technical Challenges, Recent Advances, and Future Trends, *Proceedings of the IEEE*, *104*(9), 1727–1765, `1505.07919`.

[49] **Badawy, A.**, **Elfouly, T.**, **Khattab, T.**, **Mohamed, A. and Guizani, M.** (2016). Unleashing the Secure potential of the Wireless Physical Layer: Secret Key Generation Methods, *Physical Communication*, *19*, 1 – 10.

[50] **David, H.A. and Nagaraja, H.N.** (2003). *Order Statistics*, NJ, USA: John Wiley & Sons, Inc.

CURRICULUM VITAE

Name Surname: Semiha Koşu

Place and Date of Birth: Antalya/TURKEY/1994

E-Mail:

EDUCATION:

- **B.Sc.:** 2018, Anadolu University, Electrical and Electronics Engineering
- **M.Sc.:** 2020, Istanbul Technical University, Satellite Communication and Remote Sensing

PROFESSIONAL EXPERIENCE AND REWARDS:

- Researcher in Vodafone Future Lab Project No: ITUVF20190901P02
- ITU BAP Project No: MYL-2019-42491
- Research Assistant in ITU since December, 2019

PUBLICATIONS, PRESENTATIONS AND PATENTS ON THE THESIS:

- S. Koşu, S. Ö. Ata and L. Durak-Ata 2019. Physical Layer Security Analysis of Cooperative Mobile Communication Systems with Eavesdropper Employing MRC, *28th Signal Processing and Communications Applications Conference (SIU)*, Gaziantep, Turkey, 2020, pp. 1-4, doi: 10.1109/SIU49456.2020.9302397.
- S. Koşu, S. Ö. Ata and L. Durak-Ata 2019. On the Error Performance of Relay-Assisted Vehicular Communication Systems, *IEEE Microwave Theory and Techniques in Wireless Communications (MTTW)*, Riga, Latvia, 2019, pp. 68-71, doi: 10.1109/MTTW.2019.8897226.